A MUSTA SCHEME FOR A NON-CONSERVATIVE TWO-FLUID MODEL

SVEND TOLLAK MUNKEJORD[A,D], STEINAR EVJE[B,C] AND TORE FLÅTTEN[C,B]

ABSTRACT. We present a multi-stage centred scheme, of the kind proposed by Toro [Appl. Numer. Math. 56 (2006) 1464], for numerically resolving the simultaneous flow of two fluids through a transport pipeline. This model contains non-conservative terms in both the temporal and spatial derivatives, and an extension of the standard numerical framework for conservation laws is needed.

In this paper, we rewrite the model in an equivalent mathematical form, eliminating the non-conservative time-derivatives. This allows us to use the framework described by Parés [SIAM J. Numer. Anal. 44 (2006) 300]. We develop FORCE and MUSTA-type schemes which are consistent with Parés' formalism.

Numerical simulations demonstrate a high degree of stability of our proposed schemes. Comparisons with the Roe and Rusanov schemes indicate that convergence to near-identical solutions are obtained when the non-conservative terms are discretized with respect to the same evaluation of the path-dependent integrals. However, if the schemes are not mutually *formally path-consistent* in the sense of Parés, different converged solutions are obtained.

subject classification. 76T10, 76M12, 65M12, 35L65

key words. two-phase flow, two-fluid model, MUSTA, formally path-consistent

1. INTRODUCTION

A common way of modelling dynamic two-phase flows is by formulating balance laws for mass, momentum and energy for each phase, derived from conservation principles [35]. Such models find extensive use in the petroleum [2, 23] and nuclear [4, 38] industries.

By neglecting viscous terms, as is often done in the context of such industrial applications, one obtains a system of hyperbolic partial differential equations. In particular, the system can be written in the general form

$$\frac{\partial \boldsymbol{u}}{\partial t} + \frac{\partial \boldsymbol{f}(\boldsymbol{u})}{\partial x} + \tilde{\boldsymbol{A}}(\boldsymbol{u})\frac{\partial \tilde{\boldsymbol{v}}(\boldsymbol{u})}{\partial t} + \tilde{\boldsymbol{B}}(\boldsymbol{u})\frac{\partial \tilde{\boldsymbol{w}}(\boldsymbol{u})}{\partial x} = \boldsymbol{s}(\boldsymbol{u}), \tag{1}$$

to be solved for the unknown vector $\boldsymbol{u}(x,t) \in \mathcal{S} \subset \mathbb{R}^N$. In other words, we obtain a system of conservation laws augmented with non-conservative products and source terms. The incorporation of such terms into standard numerical schemes for conservation laws is currently an active area of research [5, 6, 33, 41].

In this respect, much focus has been given to the design of *well-balanced* schemes that properly recreate equilibria between the source and flux terms [3, 51], in particular in the context of the shallow water equations [29, 32, 50]. For two-phase flow models, the notion of well-balancedness is most naturally interpreted as the ability of the numerical scheme to maintain a pressure equilibrium under a uniform velocity field; see [1, 9].

For hyperbolic conservation laws, it is well known that the weak solutions containing discontinuities are generally not unique; additional entropy requirements must be imposed. Even further complications arise in the presence of non-conservative terms. Here the integrals needed to define weak solutions are generally dependent on the integration path chosen over a given discontinuity.

This means that for non-conservative systems, it is needed to define more precisely how such a path should be selected so that generalized Rankine–Hugoniot conditions can be posed.

Based on the definition of nonconservative products introduced in [14], Parés [33] discusses this issue in detail and also introduces a generalization of the classic concept of conservative numerical schemes. Parés originally termed such schemes *path-conservative*. Provided the schemes converge in the sense of graphs [7], the weak solutions will satisfy the generalized Rankine–Hugoniot conditions. However, this is a strong form of convergence which is often violated in practice, meaning that a perfect equivalent of the Lax–Wendroff theorem does not hold for non-conservative systems. For this reason, it was suggested in the later work [7] that the schemes described by Parés [33] should be termed *formally path-consistent* instead. Throughout this paper, we will use this latter terminology.

In order to obtain formally path-consistent schemes, our two-fluid model must be rewritten in a more suitable form. In particular, the non-conservative temporal derivatives must be eliminated from (1) to obtain a system

$$\frac{\partial \boldsymbol{u}}{\partial t} + \frac{\partial \boldsymbol{f}(\boldsymbol{u})}{\partial x} + \boldsymbol{B}(\boldsymbol{u})\frac{\partial \boldsymbol{w}(\boldsymbol{u})}{\partial x} = \boldsymbol{s}(\boldsymbol{u}), \tag{2}$$

where $\boldsymbol{B}$ and $\boldsymbol{w}$ satisfy

$$\boldsymbol{B}(\boldsymbol{u})\frac{\partial \boldsymbol{w}(\boldsymbol{u})}{\partial x} = \tilde{\boldsymbol{A}}(\boldsymbol{u})\frac{\partial \tilde{\boldsymbol{v}}(\boldsymbol{u})}{\partial t} + \tilde{\boldsymbol{B}}(\boldsymbol{u})\frac{\partial \tilde{\boldsymbol{w}}(\boldsymbol{u})}{\partial x} \tag{3}$$

for smooth solutions. This transformation, detailed in Section 2.3, allows us to construct formally path-consistent versions of some classical schemes for our two-fluid model.

In particular, we are interested in schemes that can provide upwind-type resolution of all the waves present in the system. In this respect, classical Riemann solvers like the Roe and Godunov schemes are computationally expensive, as the underlying wave structure of the model is generally not available through simple algebraic expressions [13, 19].

An interesting alternative is the multi-stage numerical method denoted as MUSTA, recently proposed by Toro [42, 43]. Here the main idea is to obtain the wave-propagation information numerically by an iterative procedure. This leads to an efficient and robust algorithm that so far has given promising results for the single-phase Euler equations [39, 42, 43]. In [26], a MUSTA scheme was proposed for a model describing two-phase mixtures.

In this paper, we investigate the method for a more general model with independent velocities and energy transfers. The contributions of this paper may be summed up as follows:

1: We rewrite the general two-fluid model in the form (2) in order to facilitate the construction of numerical schemes;

2: Specifically, we construct and assess a MUSTA-type scheme for this model.

Our paper is organized as follows: In Section 2, we discuss the two-phase flow model we will be working with. We briefly review some classic results in Section 2.2, before presenting some original results in Section 2.3. In particular, we detail the transformation that allows us to rewrite the model in the form (2).

In Section 3 we first briefly review Parés' notion of *formally path-consistent* schemes [7, 33]. We then describe a natural way of constructing formally path-consistent versions of some classical numerical schemes, including the FORCE and MUSTA schemes of Toro [40, 42], and describe the specific implementation for the two-phase flow model.

Section 4 is devoted to some numerical experiments. In particular, we are interested in the stability and accuracy of the MUSTA scheme. Finally, the main results of the paper are summarized in Section 5.

2. The two-phase flow model

The classical two-fluid model is based on balance equations for mass, momentum and energy for a gas (g) and liquid (ℓ) phase. Each phase is equipped with an equation of state (EOS):

$$p_k = p_k(\rho_k, e_k) \tag{4}$$

for $k \in \{g, \ell\}$. Furthermore, we are interested in the limit of *instantaneous pressure relaxation* between the phases, so we assume

$$p = p_g(\rho_g, e_g) = p_\ell(\rho_\ell, e_\ell). \tag{5}$$

2.1. **The four-equation model.** If we assume no mass transfer between the phases and ignore all external forces but gravity, the mass and momentum equations may be written as follows:

$$\frac{\partial}{\partial t} (\rho_g \alpha_g) + \frac{\partial}{\partial x} (\rho_g \alpha_g v_g) = 0, \tag{6}$$

$$\frac{\partial}{\partial t} (\rho_\ell \alpha_\ell) + \frac{\partial}{\partial x} (\rho_\ell \alpha_\ell v_\ell) = 0, \tag{7}$$

$$\frac{\partial}{\partial t} (\rho_g \alpha_g v_g) + \frac{\partial}{\partial x} (\rho_g \alpha_g v_g^2) + \alpha_g \frac{\partial p}{\partial x} + \tau_i = \rho_g \alpha_g g_x, \tag{8}$$

$$\frac{\partial}{\partial t} (\rho_\ell \alpha_\ell v_\ell) + \frac{\partial}{\partial x} (\rho_\ell \alpha_\ell v_\ell^2) + \alpha_\ell \frac{\partial p}{\partial x} - \tau_i = \rho_\ell \alpha_\ell g_x, \tag{9}$$

where the interface momentum-exchange term τ_i will be discussed later. In addition, the following nomenclature is assumed:

ρ_k - density,
v_k - velocity,
α_k - volume fraction,
s_k - entropy,
e_k - internal energy,
T_k - temperature,
p - pressure common to both phases,
g_x - x-component of the gravitational acceleration.

Here the volume fractions satisfy

$$\alpha_g + \alpha_\ell = 1. \tag{10}$$

The model (6)–(9) may be used as a stand-alone dynamic model, provided that the EOS (4) may be reduced to

$$p_k(\rho_k, e_k) = p_k(\rho_k), \tag{11}$$

for instance by assuming constant entropy or temperature. This procedure has been used by many authors, see for instance [13, 19, 31].

2.2. **The six-equation model.** For many cases of interest, dynamic energy transfers become important and the system (6)–(9) should be augmented with appropriate energy-balance equations. For the special case of $\tau_i = 0$, these equations are commonly derived to satisfy the following criteria:

  C1: The system should respect conservation of total energy in the absence of external forces;
  C2: The system should support reversible thermodynamics in the absence of shocks.

The requirement C2 may be satisfied by imposing the following *entropy-convection* equations:

$$\frac{\partial}{\partial t} (\rho_k \alpha_k s_k) + \frac{\partial}{\partial x} (\rho_k \alpha_k s_k v_k) = 0, \tag{12}$$

so that global entropy is conserved for smooth solutions.

As described by Stewart and Wendroff [35], energy-balance equations are now obtained from (6)–(9) and (12), by using $\tau_i = 0$, as well as the thermodynamic differential

$$\mathrm{d}e_k = T_k \, \mathrm{d}s_k + \frac{p}{\rho_k^2} \, \mathrm{d}\rho_k. \tag{13}$$

We obtain the following equations:

$$\frac{\partial E_g}{\partial t} + \frac{\partial}{\partial x} (E_g v_g + \alpha_g v_g p) + p \frac{\partial \alpha_g}{\partial t} = \rho_g \alpha_g v_g g_x, \tag{14}$$

$$\frac{\partial E_\ell}{\partial t} + \frac{\partial}{\partial x} (E_\ell v_\ell + \alpha_\ell v_\ell p) + p \frac{\partial \alpha_\ell}{\partial t} = \rho_\ell \alpha_\ell v_\ell g_x, \tag{15}$$

where the *total phasic energy* E_k is the sum of the internal and kinetic energies of phase k:

$$E_k = \rho_k \alpha_k \left(\frac{1}{2} v_k^2 + e_k \right). \tag{16}$$

Summing (14) and (15) yields an equation for the total energy that satisfies C1.

2.2.1. *Phase-interaction terms.* The considerations above lead to a formulation of the energy equations for the special case $\tau_i = 0$. However, when the momentum-transfer term is present, it must also be accounted for in the energy equations. For C1 to continue to hold, (14) and (15) are then most generally expressed as:

$$\frac{\partial E_{\mathrm{g}}}{\partial t} + \frac{\partial}{\partial x} \left(E_{\mathrm{g}} v_{\mathrm{g}} + \alpha_{\mathrm{g}} v_{\mathrm{g}} p \right) + p \frac{\partial \alpha_{\mathrm{g}}}{\partial t} + v_\tau \cdot \tau_{\mathrm{i}} = \rho_{\mathrm{g}} \alpha_{\mathrm{g}} v_{\mathrm{g}} g_x, \tag{17}$$

$$\frac{\partial E_\ell}{\partial t} + \frac{\partial}{\partial x} \left(E_\ell v_\ell + \alpha_\ell v_\ell p \right) + p \frac{\partial \alpha_\ell}{\partial t} - v_\tau \cdot \tau_{\mathrm{i}} = \rho_\ell \alpha_\ell v_\ell g_x, \tag{18}$$

where we only assume that v_τ is some operator with the dimensions of a velocity. A more precise description of this operator may be obtained through entropy considerations. Here we will find it convenient to use the shorthand

$$\tau_{\mathrm{g}} = -\tau_{\mathrm{i}}, \tag{19}$$

$$\tau_\ell = \tau_{\mathrm{i}}. \tag{20}$$

It will also be convenient to work with the *material derivative* defined as

$$\frac{D\Phi_k}{Dt} = \frac{\partial \Phi_k}{\partial t} + v_k \frac{\partial \Phi_k}{\partial x}, \tag{21}$$

for any phase k and variable Φ.

The momentum-exchange term τ_i now appears as an entropy-source term, as is made precise by the following lemma:

Lemma 1. *The energy equations* (17) *and* (18) *can be expressed as*

$$\frac{\partial}{\partial t} \left(\rho_k \alpha_k s_k \right) + \frac{\partial}{\partial x} \left(\rho_k \alpha_k s_k v_k \right) = \frac{1}{T_k} \left(v_\tau - v_k \right) \tau_k. \tag{22}$$

Proof. The model (6)–(9), (17)–(18) can be expressed in terms of the material derivative as

$$\alpha_k \frac{D\rho_k}{Dt} = -\rho_k \left(\frac{\partial \alpha_k}{\partial t} + \frac{\partial}{\partial x} (\alpha_k v_k) \right), \tag{23}$$

$$\rho_k \alpha_k \frac{Dv_k}{Dt} + \alpha_k \frac{\partial p}{\partial x} - \tau_k = \rho_k \alpha_k g_x, \tag{24}$$

$$\rho_k \alpha_k \frac{D}{Dt} \left(e_k + \frac{1}{2} v_k^2 \right) + \frac{\partial (\alpha_k v_k p)}{\partial x} + p \frac{\partial \alpha_k}{\partial t} - v_\tau \tau_k = \rho_k \alpha_k v_k g_x. \tag{25}$$

Multiplying (24) with v_k and subtracting from (25) we obtain

$$\rho_k \alpha_k \frac{De_k}{Dt} = -p \frac{\partial (\alpha_k v_k)}{\partial x} - p \frac{\partial \alpha_k}{\partial t} - (v_k - v_\tau) \tau_k. \tag{26}$$

By (23) and (26), it follows from the differential relation (13) that

$$\rho_k \alpha_k \frac{Ds_k}{Dt} = \frac{1}{T_k} (v_\tau - v_k) \tau_k. \tag{27}$$

From this, (22) follows from the mass conservation equations (6)–(7).

$\square$

2.2.2. *Entropy considerations.* We first note that if the momentum-exchange term τ_i satisfies

$$(v_g - v_\ell)\tau_i \geq 0, \tag{28}$$

then momentum transfer will be positive for the faster phase and negative for the slower; hence this term will have the effect of *reducing* $|v_g - v_\ell|$, as can be seen from (8) and (9). This motivates the following definition:

Definition 1. *The momentum-exchange term τ_i will be denoted as an* **interface friction** *provided that (28) is satisfied.*

We now consider a *closed* region R and define the total cross-sectional entropy ω:

$$\omega(x, t) = \rho_g \alpha_g s_g + \rho_\ell \alpha_\ell s_\ell. \tag{29}$$

We further define the global entropy Ω:

$$\Omega(t) = \int_R \omega(x, t)\, dx. \tag{30}$$

Following [35], we now insist that the energy-transfer term must be chosen such that interface friction is consistent with the second law of thermodynamics. In particular, we have the following proposition:

Proposition 1. *If τ_i is an interface friction, the second law of thermodynamics*

$$\frac{d\Omega}{dt} \geq 0 \quad \forall t \tag{31}$$

holds if v_τ is a scalar, convex combination of v_g and v_ℓ, i.e.

$$\min(v_g, v_\ell) \leq v_\tau \leq \max(v_g, v_\ell), \tag{32}$$

or equivalently

$$v_\tau = \beta v_g + (1 - \beta)v_\ell, \quad \beta \in [0, 1]. \tag{33}$$

Proof. By (29)–(30) and Lemma 1, we have

$$\frac{d\Omega}{dt} = \int_R \left(\frac{1}{T_\ell}(v_\tau - v_\ell) - \frac{1}{T_g}(v_\tau - v_g) \right) \tau_i\, dx. \tag{34}$$

Now (31) holds if

$$\left(\frac{1}{T_\ell}(v_\tau - v_\ell) - \frac{1}{T_g}(v_\tau - v_g) \right) \tau_i \geq 0. \tag{35}$$

Substituting (33) into (35) yields

$$\left(\frac{\beta}{T_\ell} + \frac{1 - \beta}{T_g} \right) (v_g - v_\ell)\tau_i \geq 0, \tag{36}$$

which by (28) and positivity of temperatures holds for all $\beta \in [0, 1]$. $\qquad\square$

We will propose an explicit choice of β in Section 2.3.1.

2.3. **Canonical non-conservative form.** By the analysis above, we recover a rather standard formulation of the two-fluid model that has been used by several authors [12, 20, 21, 31, 35]. If we assume $\tau_i = \tau_i(\boldsymbol{u})$, the model is in the form (1):

$$\frac{\partial \boldsymbol{u}}{\partial t} + \frac{\partial \boldsymbol{f}(\boldsymbol{u})}{\partial x} + \tilde{\boldsymbol{A}}(\boldsymbol{u})\frac{\partial \tilde{\boldsymbol{v}}(\boldsymbol{u})}{\partial t} + \tilde{\boldsymbol{B}}(\boldsymbol{u})\frac{\partial \tilde{\boldsymbol{w}}(\boldsymbol{u})}{\partial x} = \boldsymbol{s}(\boldsymbol{u}), \tag{37}$$

with

$$\boldsymbol{u} = \begin{bmatrix} \rho_g \alpha_g \\ \rho_\ell \alpha_\ell \\ \rho_g \alpha_g v_g \\ \rho_\ell \alpha_\ell v_\ell \\ E_g \\ E_\ell \end{bmatrix}, \quad \boldsymbol{f}(\boldsymbol{u}) = \begin{bmatrix} \rho_g \alpha_g v_g \\ \rho_\ell \alpha_\ell v_\ell \\ \rho_g \alpha_g v_g^2 \\ \rho_\ell \alpha_\ell v_\ell^2 \\ (E_g + \alpha_g p)v_g \\ (E_\ell + \alpha_\ell p)v_\ell \end{bmatrix}, \quad \boldsymbol{s}(\boldsymbol{u}) = \begin{bmatrix} 0 \\ 0 \\ \rho_g \alpha_g g_x - \tau_i \\ \rho_\ell \alpha_\ell g_x + \tau_i \\ \rho_g \alpha_g v_g g_x - v_\tau \tau_i \\ \rho_\ell \alpha_\ell v_\ell g_x + v_\tau \tau_i \end{bmatrix}, \tag{38}$$

and

$$\tilde{\boldsymbol{A}}(\boldsymbol{u}) = p\boldsymbol{I}, \quad \tilde{\boldsymbol{v}}(\boldsymbol{u}) = \begin{bmatrix} 0 \\ 0 \\ 0 \\ 0 \\ \alpha_{\mathrm{g}} \\ \alpha_\ell \end{bmatrix}, \qquad \tilde{\boldsymbol{B}}(\boldsymbol{u}) = \begin{bmatrix} 0 \\ 0 \\ \alpha_{\mathrm{g}} \\ \alpha_\ell \\ 0 \\ 0 \end{bmatrix}, \quad \tilde{\boldsymbol{w}}(\boldsymbol{u}) = p. \tag{39}$$

In this section, we perform the transformation needed to put the model in the form (2):

$$\frac{\partial \boldsymbol{u}}{\partial t} + \frac{\partial \boldsymbol{f}(\boldsymbol{u})}{\partial x} + \boldsymbol{B}(\boldsymbol{u})\frac{\partial \boldsymbol{w}(\boldsymbol{u})}{\partial x} = \boldsymbol{s}(\boldsymbol{u}). \tag{40}$$

We begin by obtaining a useful differential.

Lemma 2. *For a general equation of state in the form*

$$p = p(\rho, e), \tag{41}$$

the pressure differential $\mathrm{d}p$ *may be expressed as*

$$\mathrm{d}p = \left(c^2 - \gamma\frac{p}{\rho}\right)\mathrm{d}\rho + \gamma\rho\,\mathrm{d}e, \tag{42}$$

where c *is the sound velocity given by*

$$c^2 = \left(\frac{\partial p}{\partial \rho}\right)_s \tag{43}$$

and γ *here is the* **first Grüneisen parameter**

$$\gamma \equiv \frac{1}{\rho C_v}\left(\frac{\partial p}{\partial T}\right)_\rho, \tag{44}$$

where C_v *is the heat capacity at constant volume given by*

$$C_v = \left(\frac{\partial e}{\partial T}\right)_v. \tag{45}$$

Proof.

$$\mathrm{d}p = \left(\frac{\partial p}{\partial \rho}\right)_s \mathrm{d}\rho + \left(\frac{\partial p}{\partial s}\right)_\rho \mathrm{d}s = c^2\,\mathrm{d}\rho + \left(\frac{\partial p}{\partial s}\right)_\rho \mathrm{d}s. \tag{46}$$

Furthermore,

$$\left(\frac{\partial p}{\partial s}\right)_\rho = \left(\frac{\partial T}{\partial s}\right)_\rho \left(\frac{\partial p}{\partial T}\right)_\rho = \frac{T}{C_v} \cdot \rho C_v \gamma = \gamma\rho T, \tag{47}$$

so that (46) may be written as

$$\mathrm{d}p = c^2\,\mathrm{d}\rho + \gamma\rho T\,\mathrm{d}s. \tag{48}$$

By substitution of the fundamental differential (13) for $\mathrm{d}s$ in (48), the lemma follows.

$\square$

We are now in a position to state the following:

Proposition 2. *The evolution equation for* α_ℓ *can be written as:*

$$\sigma\frac{\partial \alpha_\ell}{\partial t} = \rho_{\mathrm{g}}\alpha_\ell c_{\mathrm{g}}^2\frac{\partial}{\partial x}\left(\alpha_{\mathrm{g}}v_{\mathrm{g}}\right) - \rho_\ell\alpha_{\mathrm{g}}c_\ell^2\frac{\partial}{\partial x}\left(\alpha_\ell v_\ell\right) + \alpha_{\mathrm{g}}\alpha_\ell(v_{\mathrm{g}} - v_\ell)\frac{\partial p}{\partial x}$$
$$- \tau_i\left(\alpha_\ell\gamma_{\mathrm{g}}(v_{\mathrm{g}} - v_\tau) + \alpha_{\mathrm{g}}\gamma_\ell(v_\ell - v_\tau)\right), \quad (49)$$

where

$$\sigma = \alpha_{\mathrm{g}}\rho_\ell c_\ell^2 + \alpha_\ell\rho_{\mathrm{g}}c_{\mathrm{g}}^2. \tag{50}$$

Proof. We write the differential (42) as

$$\alpha_k \frac{Dp}{Dt} = \left(c_k^2 - \frac{\gamma_k p}{\rho_k} \right) \alpha_k \frac{D\rho_k}{Dt} + \gamma_k \alpha_k \rho_k \frac{De_k}{Dt}. \tag{51}$$

By (23) and (26), this simplifies to

$$\alpha_k \frac{Dp}{Dt} = -\rho_k c_k^2 \frac{\partial \alpha_k}{\partial t} - \rho_k c_k^2 \frac{\partial (\alpha_k v_k)}{\partial x} - \gamma_k (v_k - v_\tau) \tau_k. \tag{52}$$

Now writing the equations (52) for $k = \mathrm{g}$, $k = \ell$, and taking into account that

$$\frac{\partial \alpha_\mathrm{g}}{\partial t} + \frac{\partial \alpha_\ell}{\partial t} = 0, \tag{53}$$

we recover (49) by eliminating $\partial_t p$.

$\square$

2.3.1. *The interface velocity v_τ.* We now revisit the modelling of the interface-velocity operator v_τ, described in Section 2.2.2. By energy conservation, the kinetic energy released by any interface friction will be transformed into a combination of *deformation* and *heat.* We are now able to state the following proposition:

Proposition 3. *If the interface-velocity operator v_τ is modelled as*

$$v_\tau = \frac{\alpha_\ell \gamma_\mathrm{g} v_\mathrm{g} + \alpha_\mathrm{g} \gamma_\ell v_\ell}{\alpha_\ell \gamma_\mathrm{g} + \alpha_\mathrm{g} \gamma_\ell}, \tag{54}$$

i.e. in the context of (33):

$$\beta = \frac{\alpha_\ell \gamma_\mathrm{g}}{\alpha_\ell \gamma_\mathrm{g} + \alpha_\mathrm{g} \gamma_\ell}, \tag{55}$$

we get:

$$\frac{\partial}{\partial \tau_\mathrm{i}} \left(\frac{\partial \rho_k}{\partial t} \right) = 0. \tag{56}$$

In other words, there is no deformation associated with τ_i, and the kinetic energy released by the interface friction τ_i will therefore be fully converted into heat.

Proof. From (49) we have

$$\frac{\partial}{\partial \tau_\mathrm{i}} \left(\frac{\partial \alpha_\ell}{\partial t} \right) = \frac{-\left(\alpha_\ell \gamma_\mathrm{g} (v_\mathrm{g} - v_\tau) + \alpha_\mathrm{g} \gamma_\ell (v_\ell - v_\tau) \right)}{\sigma}. \tag{57}$$

With (54), this simply becomes

$$\frac{\partial}{\partial \tau_\mathrm{i}} \left(\frac{\partial \alpha_\ell}{\partial t} \right) = 0. \tag{58}$$

Then

$$\frac{\partial}{\partial \tau_\mathrm{i}} \left(\frac{\partial \rho_k}{\partial t} \right) = \frac{\partial}{\partial \tau_\mathrm{i}} \left(\frac{1}{\alpha_k} \frac{\partial}{\partial t} (\rho_k \alpha_k) - \frac{\rho_k}{\alpha_k} \frac{\partial \alpha_k}{\partial t} \right) = 0, \tag{59}$$

where we have used that the mass equations (6) and (7) are independent of τ_i.

$\square$

Note that (54) satisfies the convexity requirement (33) as both the volume fractions and Grüneisen parameters are non-negative, when we assume well-behaved thermodynamics. Hence for the purpose of this paper, we will use (54) to model the interface-velocity term in the energy equations. Although we do not claim that this is generally the most realistic choice, it has the advantage of having a direct physical interpretation.

2.3.2. *The interface momentum-exchange term τ_i.* The model (37)–(39), with the interpretation that $\tau_i = \tau_i(\boldsymbol{u})$ represents some interface friction, is sometimes referred to as the *basic equal-pressure model* [35]. It is a well-known fact that this particular model predicts complex velocities for the volume-fraction waves, meaning that unbounded instabilities are expected at short wavelengths [24, 35]. In this case, the equations do not have a well-defined mathematical solution.

Hence a common approach is to include differential terms in the modelling of τ_i in order to render the system hyperbolic with real eigenvalues. We may write

$$\tau_i = \tau_D + \tau_F, \tag{60}$$

where τ_D represents the added differential terms and $\tau_F = \tau_F(\boldsymbol{u})$. Note that τ_D does not necessarily have to satisfy (28). In particular, it has become more or less a standard for numerical testing [11, 13, 16, 31, 44] to let τ_D represent the effect of a pressure jump Δp at the gas-liquid interface. In this case, τ_D becomes:

$$\tau_D = -\Delta p \frac{\partial \alpha_\ell}{\partial x}. \tag{61}$$

Physically, Δp could represent the effects of hydrostatics or surface tension. However, we here follow previous works [9, 16, 27, 31] and use:

$$\Delta p = \delta \frac{\alpha_{\mathrm{g}} \alpha_\ell \rho_{\mathrm{g}} \rho_\ell}{\rho_{\mathrm{g}} \alpha_\ell + \rho_\ell \alpha_{\mathrm{g}}} (v_{\mathrm{g}} - v_\ell)^2, \tag{62}$$

which is motivated purely from mathematical considerations; here $\delta > 1$ ensures a hyperbolic model unless the velocity difference $v_{\mathrm{g}} - v_\ell$ becomes too large [4, 36]. In this paper, we assume

$$\delta = 1.2 \tag{63}$$

unless otherwise stated.

2.3.3. *The rewritten model.* The results of this section lead us to the following proposition:

Proposition 4. *If we choose*

$$v_\tau = \frac{\alpha_\ell \gamma_{\mathrm{g}} v_{\mathrm{g}} + \alpha_{\mathrm{g}} \gamma_\ell v_\ell}{\alpha_\ell \gamma_{\mathrm{g}} + \alpha_{\mathrm{g}} \gamma_\ell} \tag{64}$$

and

$$\tau_{\mathrm{i}} = -\Delta p \frac{\partial \alpha_\ell}{\partial x} + \tau_F(\boldsymbol{u}), \tag{65}$$

the model given by (6)–(9) and (17)–(18) can be expressed in the mathematically equivalent form

$$\frac{\partial \boldsymbol{u}}{\partial t} + \frac{\partial \boldsymbol{f}(\boldsymbol{u})}{\partial x} + \boldsymbol{B}(\boldsymbol{u}) \frac{\partial \boldsymbol{w}(\boldsymbol{u})}{\partial x} = \boldsymbol{s}(\boldsymbol{u}), \tag{66}$$

with

$$\boldsymbol{u} = \begin{bmatrix} \rho_{\mathrm{g}} \alpha_{\mathrm{g}} \\ \rho_\ell \alpha_\ell \\ \rho_{\mathrm{g}} \alpha_{\mathrm{g}} v_{\mathrm{g}} \\ \rho_\ell \alpha_\ell v_\ell \\ E_{\mathrm{g}} \\ E_\ell \end{bmatrix}, \quad \boldsymbol{f}(\boldsymbol{u}) = \begin{bmatrix} \rho_{\mathrm{g}} \alpha_{\mathrm{g}} v_{\mathrm{g}} \\ \rho_\ell \alpha_\ell v_\ell \\ \rho_{\mathrm{g}} \alpha_{\mathrm{g}} v_{\mathrm{g}}^2 + \alpha_{\mathrm{g}} \Delta p \\ \rho_\ell \alpha_\ell v_\ell^2 + \alpha_\ell \Delta p \\ (E_{\mathrm{g}} + \alpha_{\mathrm{g}} p) v_{\mathrm{g}} \\ (E_\ell + \alpha_\ell p) v_\ell \end{bmatrix}, \quad \boldsymbol{s}(\boldsymbol{u}) = \begin{bmatrix} 0 \\ 0 \\ \rho_{\mathrm{g}} \alpha_{\mathrm{g}} g_x - \tau_F \\ \rho_\ell \alpha_\ell g_x + \tau_F \\ \rho_{\mathrm{g}} \alpha_{\mathrm{g}} v_{\mathrm{g}} g_x - v_\tau \tau_F \\ \rho_\ell \alpha_\ell v_\ell g_x + v_\tau \tau_F \end{bmatrix}, \tag{67}$$

and

$$\boldsymbol{B}(\boldsymbol{u}) = \begin{bmatrix} 0 & 0 & 0 & 0 & 0 \\ 0 & 0 & 0 & 0 & 0 \\ \alpha_{\mathrm{g}} & 0 & 0 & 0 & -\alpha_{\mathrm{g}} \\ \alpha_\ell & 0 & 0 & 0 & -\alpha_\ell \\ -\eta \alpha_{\mathrm{g}} \alpha_\ell (v_{\mathrm{g}} - v_\ell) & -v_\tau \Delta p & -\eta \rho_{\mathrm{g}} \alpha_\ell c_{\mathrm{g}}^2 & \eta \rho_\ell \alpha_{\mathrm{g}} c_\ell^2 & 0 \\ \eta \alpha_{\mathrm{g}} \alpha_\ell (v_{\mathrm{g}} - v_\ell) & v_\tau \Delta p & \eta \rho_{\mathrm{g}} \alpha_\ell c_{\mathrm{g}}^2 & -\eta \rho_\ell \alpha_{\mathrm{g}} c_\ell^2 & 0 \end{bmatrix}, \quad \boldsymbol{w}(\boldsymbol{u}) = \begin{bmatrix} p \\ \alpha_\ell \\ \alpha_{\mathrm{g}} v_{\mathrm{g}} \\ \alpha_\ell v_\ell \\ \Delta p \end{bmatrix}, \tag{68}$$

where

$$\eta = \frac{p}{\sigma} = \frac{p}{\alpha_{\mathrm{g}} \rho_\ell c_\ell^2 + \alpha_\ell \rho_{\mathrm{g}} c_{\mathrm{g}}^2}. \tag{69}$$

Proof. From (49) and (64) we get

$$\sigma \frac{\partial \alpha_\ell}{\partial t} = \rho_{\mathrm{g}} \alpha_\ell c_{\mathrm{g}}^2 \frac{\partial}{\partial x} (\alpha_{\mathrm{g}} v_{\mathrm{g}}) - \rho_\ell \alpha_{\mathrm{g}} c_\ell^2 \frac{\partial}{\partial x} (\alpha_\ell v_\ell) + \alpha_{\mathrm{g}} \alpha_\ell (v_{\mathrm{g}} - v_\ell) \frac{\partial p}{\partial x}. \tag{70}$$

Substitute this for $\partial_t \alpha$ in the energy equations (17)–(18), using $\partial_t \alpha_{\mathrm{g}} = -\partial_t \alpha_\ell$. Furthermore, substitute (65) in (8)–(9) and (17)–(18), and the result follows. □

For practical simulations, further terms may be added to the framework (66)–(69), for instance mass-transfer terms or heat-transfer terms; see [4, 35]. Aiming for simplicity, we here follow previous authors [9, 11, 12, 31, 44] and neglect such terms for the purpose of numerical benchmarking.

2.3.4. *Canonical non-conservative form of the four-equation model.* We may also write the simpler four-equation model (6)–(9) in the form (66); we obtain

$$\boldsymbol{u} = \begin{bmatrix} \rho_{\mathrm{g}} \alpha_{\mathrm{g}} \\ \rho_\ell \alpha_\ell \\ \rho_{\mathrm{g}} \alpha_{\mathrm{g}} v_{\mathrm{g}} \\ \rho_\ell \alpha_\ell v_\ell \end{bmatrix}, \quad \boldsymbol{f}(\boldsymbol{u}) = \begin{bmatrix} \rho_{\mathrm{g}} \alpha_{\mathrm{g}} v_{\mathrm{g}} \\ \rho_\ell \alpha_\ell v_\ell \\ \rho_{\mathrm{g}} \alpha_{\mathrm{g}} v_{\mathrm{g}}^2 + \alpha_{\mathrm{g}} \Delta p \\ \rho_\ell \alpha_\ell v_\ell^2 + \alpha_\ell \Delta p \end{bmatrix}, \quad \boldsymbol{s}(\boldsymbol{u}) = \begin{bmatrix} 0 \\ 0 \\ \rho_{\mathrm{g}} \alpha_{\mathrm{g}} g_x - \tau_F \\ \rho_\ell \alpha_\ell g_x + \tau_F \end{bmatrix}, \tag{71}$$

and

$$\boldsymbol{B}(\boldsymbol{u}) = \begin{bmatrix} 0 \\ 0 \\ \alpha_{\mathrm{g}} \\ \alpha_\ell \end{bmatrix}, \quad \boldsymbol{w}(\boldsymbol{u}) = p - \Delta p. \tag{72}$$

3. NUMERICAL SCHEMES

The model formulation (66)–(69) now allows us to use the framework described by Parés [33]. Parés considered the general non-conservative problem:

$$\frac{\partial \boldsymbol{u}}{\partial t} + \boldsymbol{A}(\boldsymbol{u}) \frac{\partial \boldsymbol{u}}{\partial x} = \boldsymbol{0}, \tag{73}$$

where the vector $\boldsymbol{u}(x, t)$ belongs to an open subset $\mathcal{S}$ of $\mathbb{R}^N$. Consider now a discontinuity between two states $\boldsymbol{u}_{\mathrm{L}}$ and $\boldsymbol{u}_{\mathrm{R}}$, connected by a family of paths $\Psi(s; \boldsymbol{u}_{\mathrm{L}}, \boldsymbol{u}_{\mathrm{R}})$. Certain consistency requirements are needed for such families of paths, we here restate Parés' definition:

Definition 2. *A family of paths in $\mathcal{S} \subset \mathbb{R}^N$ is a locally Lipschitz map*

$$\Psi : [0, 1] \times \mathcal{S} \times \mathcal{S} \to \mathcal{S}, \tag{74}$$

such that:
- $\Psi(0; \boldsymbol{u}_{\mathrm{L}}, \boldsymbol{u}_{\mathrm{R}}) = \boldsymbol{u}_{\mathrm{L}}$ *and* $\Psi(1; \boldsymbol{u}_{\mathrm{L}}, \boldsymbol{u}_{\mathrm{R}}) = \boldsymbol{u}_{\mathrm{R}}$, *for any* $\boldsymbol{u}_{\mathrm{L}}, \boldsymbol{u}_{\mathrm{R}} \in \mathcal{S}$;
- *for every arbitrary bounded set* $\mathcal{O} \subset \mathcal{S}$, *there exists a constant k such that*

$$\left| \frac{\partial \Psi}{\partial s}(s; \boldsymbol{u}_{\mathrm{L}}, \boldsymbol{u}_{\mathrm{R}}) \right| \le k |\boldsymbol{u}_{\mathrm{R}} - \boldsymbol{u}_{\mathrm{L}}|, \tag{75}$$

  for any $\boldsymbol{u}_{\mathrm{L}}, \boldsymbol{u}_{\mathrm{R}} \in \mathcal{O}$ *and almost every* $s \in [0, 1]$;
- *for every bounded set* $\mathcal{O} \in \mathcal{S}$, *there exists a constant K such that*

$$\left| \frac{\partial \Psi}{\partial s}(s; \boldsymbol{u}_{\mathrm{L}}^1, \boldsymbol{u}_{\mathrm{R}}^1) - \frac{\partial \Psi}{\partial s}(s; \boldsymbol{u}_{\mathrm{L}}^2, \boldsymbol{u}_{\mathrm{R}}^2) \right| \le K(|\boldsymbol{u}_{\mathrm{L}}^1 - \boldsymbol{u}_{\mathrm{L}}^2| + |\boldsymbol{u}_{\mathrm{R}}^1 - \boldsymbol{u}_{\mathrm{R}}^2|), \tag{76}$$

  for any $\boldsymbol{u}_{\mathrm{L}}^1, \boldsymbol{u}_{\mathrm{R}}^1, \boldsymbol{u}_{\mathrm{L}}^2, \boldsymbol{u}_{\mathrm{R}}^2 \in \mathcal{O}$ *and almost every* $s \in [0, 1]$.

One may then state a *generalized Rankine–Hugoniot* condition for the propagation velocity ξ of such discontinuities in non-conservative systems:

$$\int_0^1 (\xi \boldsymbol{I} - \boldsymbol{A}(\Psi(s; \boldsymbol{u}_{\mathrm{L}}, \boldsymbol{u}_{\mathrm{R}}))) \frac{\partial \Psi}{\partial s}(s; \boldsymbol{u}_{\mathrm{L}}, \boldsymbol{u}_{\mathrm{R}}) \, \mathrm{d}s = 0. \tag{77}$$

Now ξ is independent of the choice of the family of paths only when $\boldsymbol{A}(\boldsymbol{u})$ is the Jacobian of some flux function $\boldsymbol{f}(\boldsymbol{u})$; in this case, (77) reduces to the usual Rankine–Hugoniot condition.

Hence a weak solution to a non-conservative system cannot be defined without the specification of some family of paths Ψ. However, given such a choice of Ψ, Parés [33] discusses the construction of numerical schemes that in a certain sense respect the generalized Rankine–Hugoniot condition (77); such schemes are referred to as *formally Ψ-consistent* [7].

3.1. **Formally Path-consistent schemes.** Following Parés [33, 7], we may state the following definition:

Definition 3. *Given a family of paths Ψ, a numerical scheme for the equation* (73) *is said to be formally Ψ-consistent if it can be written in the form*

$$\boldsymbol{u}_j^{n+1} = \boldsymbol{u}_j^n - \frac{\Delta t}{\Delta x}(\boldsymbol{D}_{j-1/2}^+ + \boldsymbol{D}_{j+1/2}^-), \tag{78}$$

where

$$\boldsymbol{D}_{j+1/2}^\pm = \boldsymbol{D}^\pm(\boldsymbol{u}_{j-q}^n, \ldots, \boldsymbol{u}_{j+p}^n), \tag{79}$$

$\boldsymbol{D}^-$ *and* $\boldsymbol{D}^+$ *being two continuous functions from* $\mathcal{S}^{p+q+1}$ *to* $\mathcal{S}$ *satisfying:*

$$\boldsymbol{D}^\pm(\boldsymbol{u}, \ldots, \boldsymbol{u}) = 0 \qquad \forall \boldsymbol{u} \in \mathcal{S}, \tag{80}$$

and

$$\boldsymbol{D}^-(\boldsymbol{u}_{-q}, \ldots, \boldsymbol{u}_p) + \boldsymbol{D}^+(\boldsymbol{u}_{-q}, \ldots, \boldsymbol{u}_p) = \int_0^1 \boldsymbol{A}(\Psi(s; \boldsymbol{u}_0, \boldsymbol{u}_1))\frac{\partial \Psi}{\partial s}(s; \boldsymbol{u}_0, \boldsymbol{u}_1)\,\mathrm{d}s, \tag{81}$$

for every choice of $\boldsymbol{u}_i \in \mathcal{S}$, $i = -q, \ldots, p$.

Furthermore, Parés [33] proves the following proposition:

Proposition 5. *Let us suppose that* (73) *is a system of conservation laws; i.e.* $\boldsymbol{A}$ *is the Jacobian of some flux function* $\boldsymbol{f}$. *Then, every numerical scheme which is formally Ψ-consistent for some family of paths Ψ is consistent and conservative in the usual sense. Conversely, a consistent conservative numerical scheme is formally Ψ-consistent for every family of paths Ψ.*

Hence the class of *conservative* numerical schemes for conservation laws is a special case of the more general class of *formally path-consistent* numerical schemes.

To obtain a numerical scheme, one now needs to complete the followings tasks:

(1) Select a particular family of paths Ψ;
(2) Evaluate the path-dependent integrals (81).

In general, the choice of the family of paths should be based on physical considerations applied to the given problem. Furthermore, useful results can be formally proved [28] when the family of paths satisfies certain properties related to the integral curves linking the states $\boldsymbol{u}_{\mathrm{L}}$ and $\boldsymbol{u}_{\mathrm{R}}$.

However, in the context of our two-fluid model it is not clear how to select a physical path, as the eigenstructure of the model cannot be expressed in terms of simple analytical expressions [13, 16, 44]. And even equipped with a choice of family of paths Ψ, it remains a nontrivial task to compute the path-dependent integrals (81).

In the following section, we will discuss how the evaluation of the non-conservative integrals and the construction of formally path-consistent numerical schemes can be treated as independent problems.

3.1.1. *A simplified framework.* Now let

$$\boldsymbol{A}(\boldsymbol{u}) \equiv \frac{\partial \boldsymbol{f}(\boldsymbol{u})}{\partial \boldsymbol{u}} + \boldsymbol{B}(\boldsymbol{u})\frac{\partial \boldsymbol{w}}{\partial \boldsymbol{u}}, \tag{82}$$

so that (66) can be written as:

$$\frac{\partial \boldsymbol{u}}{\partial t} + \boldsymbol{A}(\boldsymbol{u})\frac{\partial \boldsymbol{u}}{\partial x} = \boldsymbol{s}(\boldsymbol{u}). \tag{83}$$

Here the function $\boldsymbol{w}(\boldsymbol{u}) \in \mathcal{T}$ is a smooth mapping from $\mathcal{S}$ to a subset $\mathcal{T}$ of $\mathbb{R}^M$.

Let us assume that a family of paths Ψ has been chosen. This naturally defines a corresponding set of points in $\mathcal{T}$ through the mapping:

$$\Phi : [0, 1] \times \mathcal{S} \times \mathcal{S} \to \mathcal{T}, \tag{84}$$

given by

$$\Phi(s; \boldsymbol{u}_j, \boldsymbol{u}_{j+1}) = \boldsymbol{w}(\Psi(s; \boldsymbol{u}_j, \boldsymbol{u}_{j+1})). \tag{85}$$

In the following, we will use the shorthand

$$\boldsymbol{w}_j = \boldsymbol{w}(\boldsymbol{u}_j). \tag{86}$$

Now define a *cell-interface* value $\boldsymbol{B}_{j+1/2}$ as an average satisfying

$$
\begin{aligned}
\boldsymbol{B}_{j+1/2}\left(\boldsymbol{w}_{j+1} - \boldsymbol{w}_j\right) &= \int_0^1 \boldsymbol{B}(\Psi(s; \boldsymbol{u}_j, \boldsymbol{u}_{j+1}))\frac{\partial \Phi}{\partial s}(s; \boldsymbol{u}_j, \boldsymbol{u}_{j+1})\,\mathrm{d}s \\
&= \int_0^1 \left(\boldsymbol{B} \cdot \frac{\partial \boldsymbol{w}}{\partial \boldsymbol{u}}\right)(\Psi(s; \boldsymbol{u}_j, \boldsymbol{u}_{j+1}))\frac{\partial \Psi}{\partial s}(s; \boldsymbol{u}_j, \boldsymbol{u}_{j+1})\,\mathrm{d}s.
\end{aligned}
\tag{87}
$$

Furthermore, let $\boldsymbol{f}_{j+1/2}^n$ and $\boldsymbol{w}_{j+1/2}^n$ be consistent approximations to $\boldsymbol{f}(x_{j+1/2}, t^n)$ and $\boldsymbol{w}(x_{j+1/2}, t^n)$ in the following sense:

C1: $\boldsymbol{w}_{j+1/2}(\boldsymbol{u}_{j-q}, \ldots, \boldsymbol{u}_{j+p})$ and $\boldsymbol{f}_{j+1/2}(\boldsymbol{u}_{j-q}, \ldots, \boldsymbol{u}_{j+p})$ are Lipschitz continuous functions;
C2: $\boldsymbol{w}_{j+1/2}(\boldsymbol{u}, \ldots, \boldsymbol{u}) = \boldsymbol{w}(\boldsymbol{u}), \qquad \boldsymbol{f}_{j+1/2}(\boldsymbol{u}, \ldots, \boldsymbol{u}) = \boldsymbol{f}(\boldsymbol{u}).$

We may now state the following proposition:

Proposition 6. *Given a system of balance laws in the form*

$$\frac{\partial \boldsymbol{u}}{\partial t} + \frac{\partial \boldsymbol{f}(\boldsymbol{u})}{\partial x} + \boldsymbol{B}(\boldsymbol{u})\frac{\partial \boldsymbol{w}(\boldsymbol{u})}{\partial x} = \boldsymbol{0}, \tag{88}$$

where the matrix $\boldsymbol{B}$ is a sufficiently smooth function of the vector $\boldsymbol{u}$, a scheme in the form

$$\frac{\boldsymbol{u}_j^{n+1} - \boldsymbol{u}_j^n}{\Delta t} + \frac{\boldsymbol{f}_{j+1/2} - \boldsymbol{f}_{j-1/2}}{\Delta x} + \frac{\boldsymbol{d}_{j-1/2}^+ + \boldsymbol{d}_{j+1/2}^-}{\Delta x} = \boldsymbol{0}, \tag{89}$$

where

$$\boldsymbol{d}_{j+1/2}^+ = \boldsymbol{B}_{j+1/2}\left(\boldsymbol{w}_{j+1} - \boldsymbol{w}_{j+1/2}\right) \tag{90}$$

$$\boldsymbol{d}_{j+1/2}^- = \boldsymbol{B}_{j+1/2}\left(\boldsymbol{w}_{j+1/2} - \boldsymbol{w}_j\right), \tag{91}$$

*and $\boldsymbol{f}_{j+1/2}$ and $\boldsymbol{w}_{j+1/2}$ are consistent in the sense of C1 and C2, is **formally consistent** with a family of paths Ψ, if the matrix $\boldsymbol{B}_{j+1/2}$ satisfies (87). Conversely, given an averaged matrix $\boldsymbol{B}_{j+1/2}$, the scheme is **formally consistent** with any family of paths Ψ that satisfies (87).*

Proof. Define

$$
\begin{aligned}
\boldsymbol{D}_{j+1/2}^+ &= \boldsymbol{f}(\boldsymbol{u}_{j+1}) - \boldsymbol{f}_{j+1/2} + \boldsymbol{d}_{j+1/2}^+ \tag{92} \\
\boldsymbol{D}_{j+1/2}^- &= \boldsymbol{f}_{j+1/2} - \boldsymbol{f}(\boldsymbol{u}_j) + \boldsymbol{d}_{j+1/2}^-, \tag{93}
\end{aligned}
$$

to put (89) in the form (78). Note that by (90)–(91) and C2, (92) and (93) satisfy (80).

Furthermore, by using (90)–(93) in the requirement (81), we get

$$\boldsymbol{f}(\boldsymbol{u}_{j+1}) - \boldsymbol{f}(\boldsymbol{u}_j) + \boldsymbol{B}_{j+1/2}\left(\boldsymbol{w}_{j+1} - \boldsymbol{w}_j\right) = \int_0^1 \boldsymbol{A}(\Psi(s; \boldsymbol{u}_j, \boldsymbol{u}_{j+1}))\frac{\partial \Psi}{\partial s}(s; \boldsymbol{u}_j, \boldsymbol{u}_{j+1})\,\mathrm{d}s, \tag{94}$$

or by (82):

$$
\begin{aligned}
\boldsymbol{f}(\boldsymbol{u}_{j+1}) &- \boldsymbol{f}(\boldsymbol{u}_j) + \boldsymbol{B}_{j+1/2}\left(\boldsymbol{w}_{j+1} - \boldsymbol{w}_j\right) \\
&= \int_0^1 \left(\frac{\partial \boldsymbol{f}}{\partial \boldsymbol{u}} + \boldsymbol{B} \cdot \frac{\partial \boldsymbol{w}}{\partial \boldsymbol{u}}\right)(\Psi(s; \boldsymbol{u}_j, \boldsymbol{u}_{j+1}))\frac{\partial \Psi}{\partial s}(s; \boldsymbol{u}_j, \boldsymbol{u}_{j+1})\,\mathrm{d}s, \tag{95}
\end{aligned}
$$

which simplifies to

$$\boldsymbol{B}_{j+1/2}\left(\boldsymbol{w}_{j+1} - \boldsymbol{w}_j\right) = \int_0^1 \left(\boldsymbol{B} \cdot \frac{\partial \boldsymbol{w}}{\partial \boldsymbol{u}}\right)(\Psi(s; \boldsymbol{u}_j, \boldsymbol{u}_{j+1}))\frac{\partial \Psi}{\partial s}(s; \boldsymbol{u}_j, \boldsymbol{u}_{j+1})\,\mathrm{d}s \tag{96}$$

by evaluation of the conservative part of the integral and cancellation of terms. Hence we have recovered our assumption (87), and the requirements of Definition 3 are satisfied. $\square$

The usefulness of Proposition 6 lies in the fact that once a matrix $\boldsymbol{B}_{j+1/2}$ that satisfies (87) has been found, *any* consistent discretization of $\boldsymbol{f}_{j+1/2}$ and $\boldsymbol{w}_{j+1/2}$ automatically yields a formally path-consistent scheme. This allows us to quite straightforwardly state various formally path-consistent schemes for systems in the form (66) in general, and the two-fluid model (67)–(69) in particular. This will be detailed in the following sections.

Remark 1 (upwinding). *Note that (90) and (91) properly reduce to an upwind formulation when a one-sided evaluation is used for* $\boldsymbol{w}_{j+1/2}$:

- *If* $\boldsymbol{w}_{j+1/2} = \boldsymbol{w}_j \quad \forall j$, *then*

$$\boldsymbol{d}_{j-1/2}^+ + \boldsymbol{d}_{j+1/2}^- = \boldsymbol{B}_{j-1/2}\left(\boldsymbol{w}_j - \boldsymbol{w}_{j-1}\right). \tag{97}$$

- *If* $\boldsymbol{w}_{j+1/2} = \boldsymbol{w}_{j+1} \quad \forall j$, *then*

$$\boldsymbol{d}_{j-1/2}^+ + \boldsymbol{d}_{j+1/2}^- = \boldsymbol{B}_{j+1/2}\left(\boldsymbol{w}_{j+1} - \boldsymbol{w}_j\right). \tag{98}$$

3.2. **Some classical schemes.** In this section, we describe non-conservative versions of some classical schemes for conservative systems. In particular, our non-conservative schemes will satisfy the following natural properties:

p1: The schemes should reduce to their standard conservative formulation if the coefficient matrix $\boldsymbol{B}$ is constant. More precisely, when applied to the non-conservative system

$$\frac{\partial \boldsymbol{u}}{\partial t} + \frac{\partial \boldsymbol{f}(\boldsymbol{u})}{\partial x} + \boldsymbol{B}\frac{\partial \boldsymbol{w}(\boldsymbol{u})}{\partial x} = \boldsymbol{0}, \tag{99}$$

the schemes should precisely coincide with their standard conservative formulation for the system

$$\frac{\partial \boldsymbol{u}}{\partial t} + \frac{\partial \boldsymbol{g}(\boldsymbol{u})}{\partial x} = \boldsymbol{0}, \tag{100}$$

where

$$\boldsymbol{g} \equiv \boldsymbol{f} + \boldsymbol{B}\boldsymbol{w} \tag{101}$$

whenever $\boldsymbol{B}$ is constant.

p2: The schemes should be *formally path-consistent* in the sense of Proposition 6.

De Vuyst [15] described and tested several non-conservative schemes in the context of two-phase flows. In the following, we will use his proposed schemes as a basis for constructing our formally path-consistent MUSTA scheme. We note that non-conservative versions of both the Lax-Friedrichs and the Lax-Wendroff schemes, as well as the FORCE, GFORCE and MUSTA schemes, have already been proposed by Castro *et al.* [8]. Here a slightly different strategy has been used to achieve formal path-consistency, as well as higher order-accuracy.

3.2.1. *The Lax–Friedrichs scheme.* For the non-conservative system (88), De Vuyst proposed the following Lax–Friedrichs-type discretization:

$$\boldsymbol{f}_{j+1/2}^{\mathrm{LF}} = \frac{1}{2}\left(\boldsymbol{f}(\boldsymbol{u}_j) + \boldsymbol{f}(\boldsymbol{u}_{j+1})\right) + \frac{1}{2}\frac{\Delta x}{\Delta t}\left(\boldsymbol{u}_j - \boldsymbol{u}_{j+1}\right), \tag{102}$$

$$\boldsymbol{d}_{j+1/2}^{\pm} = \frac{1}{2}\boldsymbol{B}_{j+1/2}\left(\boldsymbol{w}_{j+1} - \boldsymbol{w}_j\right) \tag{103}$$

in the context of the general scheme (89). This fits into our framework (90)–(91) if we choose

$$\boldsymbol{w}_{j+1/2}^{\mathrm{LF}} = \frac{1}{2}\left(\boldsymbol{w}_j + \boldsymbol{w}_{j+1}\right), \tag{104}$$

so that the property p2 holds. It may be easily checked that the property p1 also holds.

3.2.2. *The Rusanov scheme.* By a straightforward modification of the Lax–Friedrichs scheme, we obtain our formally path-consistent version of the Rusanov scheme:

$$\boldsymbol{f}_{j+1/2}^{\mathrm{RUS}} = \frac{1}{2}\left(\boldsymbol{f}(\boldsymbol{u}_j) + \boldsymbol{f}(\boldsymbol{u}_{j+1})\right) + \frac{S_{\mathrm{R}}}{2}\left(\boldsymbol{u}_j - \boldsymbol{u}_{j+1}\right), \tag{105}$$

$$\boldsymbol{w}_{j+1/2}^{\mathrm{RUS}} = \frac{1}{2}\left(\boldsymbol{w}_j + \boldsymbol{w}_{j+1}\right), \tag{106}$$

where

$$S_{\mathrm{R}} = \max_{1 \le p \le d}(|\lambda_j^p|, |\lambda_{j+1}^p|), \tag{107}$$

and d is the number of characteristic fields of the system.

3.2.3. *The Richtmyer scheme.* We consider the two-step Richtmyer version of the Lax–Wendroff scheme. First evolve the cell-interface solution one half time-step using a simple Lax–Friedrichs scheme:

$$\boldsymbol{u}_{j+1/2}^{n+1/2} = \frac{1}{2}\left(\boldsymbol{u}_j^n + \boldsymbol{u}_{j+1}^n\right) - \frac{\Delta t}{2\Delta x}\left(\boldsymbol{f}(\boldsymbol{u}_{j+1}^n) - \boldsymbol{f}(\boldsymbol{u}_j^n)\right) - \frac{\Delta t}{2\Delta x}\boldsymbol{B}_{j+1/2}^n\left(\boldsymbol{w}_{j+1}^n - \boldsymbol{w}_j^n\right). \tag{108}$$

Then, in the context of (89)–(91), the numerical cell-interface values are given as:

$$\boldsymbol{f}_{j+1/2}^{\mathrm{LW}} = \boldsymbol{f}(\boldsymbol{u}_{j+1/2}^{n+1/2}), \tag{109}$$

$$\boldsymbol{w}_{j+1/2}^{\mathrm{LW}} = \boldsymbol{w}(\boldsymbol{u}_{j+1/2}^{n+1/2}). \tag{110}$$

A simple check reveals that also this Richtmyer scheme satisfies the properties p1 and p2.

3.2.4. *The FORCE scheme.* The FORCE (First-ORder-CEntred) scheme has been extensively analysed by Toro and coworkers [10, 40]. It is optimal in the sense that it has the least numerical dissipation of the first-order central schemes that are stable for all CFL numbers less than unity [10].

The FORCE numerical flux is expressed as the arithmetic mean of the Richtmyer Lax–Wendroff flux and the Lax–Friedrichs flux, i.e.

$$\boldsymbol{f}_{j+1/2}^{\mathrm{FORCE}} = \frac{1}{2}\left(\boldsymbol{f}_{j+1/2}^{\mathrm{LF}} + \boldsymbol{f}_{j+1/2}^{\mathrm{LW}}\right). \tag{111}$$

The most natural choice is now to use the same averaging for the cell-interface value $\boldsymbol{w}_{j+1/2}$:

$$\boldsymbol{w}_{j+1/2}^{\mathrm{FORCE}} = \frac{1}{2}\left(\boldsymbol{w}_{j+1/2}^{\mathrm{LF}} + \boldsymbol{w}_{j+1/2}^{\mathrm{LW}}\right). \tag{112}$$

Again we may easily convince ourselves that this scheme satisfies the properties p1 and p2.

3.2.5. *The MUSTA scheme.* In the multi-stage (MUSTA) approach [39, 43], the numerical flux $\boldsymbol{f}_{j+1/2}$ at the cell interface is found by employing a two-step procedure: First, a numerical approximation to the solution of the cell-interface Riemann problem produces two modified states at either side of the interface. These states are then fed into a numerical flux function to obtain the sought flux, $\boldsymbol{f}_{j+1/2}$. There are several conceivable choices for the numerical flux function. Titarev and Toro [39] employed the FORCE flux, whereas Toro and Titarev [43] promoted a development termed the GFORCE flux. We prefer the 'classical' FORCE flux.

The MUSTA procedure employed here is similar to the previous ones for the Euler equations [39, 43] and for the drift-flux model [26], but it is extended to account for the non-conservative terms in the governing equations.

For calculating the numerical flux $\boldsymbol{f}_{j+1/2}$ and the non-conservative variables vector $\boldsymbol{w}_{j+1/2}$, the Riemann problem at the cell interface $x_{j+1/2}$ is transformed to a local grid:

$$\frac{\partial \boldsymbol{u}}{\partial t} + \frac{\partial \boldsymbol{f}(\boldsymbol{u})}{\partial \xi} + \boldsymbol{B}(\boldsymbol{u})\frac{\partial \boldsymbol{w}(\boldsymbol{u})}{\partial \xi} = \boldsymbol{0}, \qquad \boldsymbol{u}(\xi, 0) = \begin{cases} \boldsymbol{u}_j = \boldsymbol{u}_{\mathrm{L}} & \text{if } \xi < 0, \\ \boldsymbol{u}_{j+1} = \boldsymbol{u}_{\mathrm{R}} & \text{if } \xi \ge 0. \end{cases} \tag{113}$$
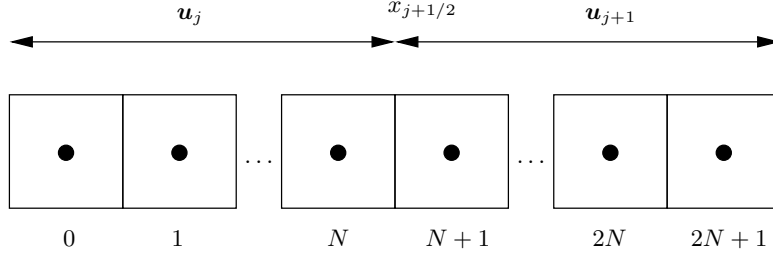
Figure 1: Initial values and cell numbering for the local MUSTA grid.

Herein, the position $\xi = 0$ corresponds to $x_{j+1/2}$. This local Riemann problem is then solved approximately by employing the FORCE scheme, where the local grid is indexed by n, and, following Titarev and Toro [39], we set $\Delta\xi \equiv \Delta x$:

$$\frac{\boldsymbol{u}_n^{m+1} - \boldsymbol{u}_n^m}{\Delta t_{\mathrm{loc}}} + \frac{\boldsymbol{f}_{n+1/2}^{\mathrm{FORCE}} - \boldsymbol{f}_{n-1/2}^{\mathrm{FORCE}}}{\Delta x} + \frac{\boldsymbol{B}_{n-1/2}(\boldsymbol{w}_n - \boldsymbol{w}_{n-1/2}^{\mathrm{FORCE}}) + \boldsymbol{B}_{n+1/2}(\boldsymbol{w}_{n+1/2}^{\mathrm{FORCE}} - \boldsymbol{w}_n)}{\Delta x} = \boldsymbol{0}.$$
(114)

Herein, $\boldsymbol{f}_{n+1/2}^{\mathrm{FORCE}}$ and $\boldsymbol{w}_{n+1/2}^{\mathrm{FORCE}}$ are calculated as described in the preceding subsections, while $\boldsymbol{w}_n = \boldsymbol{w}(\boldsymbol{u}_n)$. Terms without a time index are evaluated at stage m. Regarding the calculation of the matrix $\boldsymbol{B}_{n+1/2} = \boldsymbol{B}_{n+1/2}(\boldsymbol{u}_n, \boldsymbol{u}_{n+1})$, more details are given in Section 3.3. The local pseudo-time step Δt_{loc} is calculated using the Courant–Friedrichs–Lewy (CFL) criterion on the local grid:

$$\Delta t_{\mathrm{loc}} = \frac{r_{\mathrm{loc}}\Delta x}{\max\limits_{1 \le n \le 2N}\left(\max\limits_{1 \le p \le d}|\lambda_n^p|\right)},$$
(115)

where d is the dimension of the system (66), and the local CFL number, r_{loc}, is a parameter in the method. In this work we follow Titarev and Toro [39] and set $r_{\mathrm{loc}} = 0.9$ for all the computations. The maximum eigenvalues λ are approximated using the estimates of Evje and Flåtten [16].

The initial conditions and the numbering of the local grid are illustrated in Figure 1. The M-stage MUSTA algorithm for the flux $\boldsymbol{f}$ and the vector $\boldsymbol{w}$ can be summarized as follows:

(1) For each local cell $n = 1, \ldots, 2N$, compute the flux $\boldsymbol{f}_{n+1/2}^{\mathrm{FORCE},m}$ from (111), the vector $\boldsymbol{w}_{n+1/2}^{\mathrm{FORCE},m}$ from (112) and the coefficient matrix $\boldsymbol{B}_{n+1/2}^m$ using data from stage m.

(2) If $m = M$, then return $\boldsymbol{f}_{N+1/2}^{\mathrm{FORCE},M}$ and $\boldsymbol{w}_{N+1/2}^{\mathrm{FORCE},M}$, else continue.

(3) Update the local solution using (114) for $n = 1, \ldots, 2N$.

(4) Apply extrapolation boundary conditions; $\boldsymbol{u}_0^m = \boldsymbol{u}_1^m$ and $\boldsymbol{u}_{2N+1}^m = \boldsymbol{u}_{2N}^m$. Augment m and repeat from 1.

Thus, when the MUSTA scheme is used to solve (89)–(91), $\boldsymbol{f}_{j+1/2}$ and $\boldsymbol{w}_{j+1/2}$ are found using the above algorithm, whereas $\boldsymbol{B}_{j+1/2}$ and the other quantities are calculated using data from the global grid, as usual. This ensures that property p2 is satisfied. Furthermore, we note that the above procedure reduces to the standard conservative MUSTA algorithm [39, 43] when $\boldsymbol{B}$ is constant in time and space (property p1).

It should be noted that to avoid spurious oscillations, it is necessary to choose $M \le 2N$ in the MUSTA algorithm [26]. In the following, we will denote the M-stage MUSTA scheme with $2N$ local cells by MUSTA_{M-2N}.

It is possible to save some computational time by refining the above MUSTA algorithm. In fact, since we are solving a Riemann problem, and since we are only interested in the solution at the mid cell interface, it is not necessary to include all the local cells $n = 1, \ldots, 2N$ in all the local time steps, as noted in [39, 43]. For instance, in the first local time step, only the two mid cells enter into the calculation. In the next step, one cell has to be added at each side, as the waves propagate at most one cell per time step. When the waves have reached the boundary of the local

grid, one cell can be excluded at each side, etc. This 'diamond optimization' was suggested by Toro and Titarev [43] and has been used for all the computations presented here.

3.3. Evaluation of the cell-interface matrix $\boldsymbol{B}_{j+1/2}$.

To calculate the cell-interface matrix $\boldsymbol{B}_{j+1/2}$ from (87), we need to specify a family of integration paths, Ψ. Parés [33] discusses conditions when the path should be a parametrization of the integral curves linking the left-hand and right-hand states through the Riemann similarity solution. Since the Riemann problem for the current models has no analytical solution in general, we will instead define the family of paths *indirectly* by choosing the end result $\boldsymbol{B}_{j+1/2}$. In particular, we propose to calculate $\boldsymbol{B}_{j+1/2}$ from some appropriate average state of the cells j and $j+1$. That is,

$$\boldsymbol{B}_{j+1/2} = \boldsymbol{B}(\boldsymbol{u}_{j+1/2}). \tag{116}$$

In the context of two-phase flow, similar approaches have previously been used by Toumi and Kumbaro [45] as well as Evje and Flåtten [16].

In this paper, we will let $\boldsymbol{u}_{j+1/2}$ be given as the arithmetic average of some parameter vector $\boldsymbol{q}(\boldsymbol{u})$:

$$\boldsymbol{u}_{j+1/2} = \boldsymbol{u}(\boldsymbol{q}_{j+1/2}), \tag{117}$$

where the ith component $q_{i,j+1/2}$ of $\boldsymbol{q}_{j+1/2}$ is found by arithmetic averaging:

$$q_{i,j+1/2} = \frac{1}{2}(q_{i,j} + q_{i,j+1}). \tag{118}$$

One then sees that the definition (87) becomes a Roe-like condition on $\boldsymbol{B}_{j+1/2}$ if the value of the path integral is known. As that is not the case here, we will simply let $\boldsymbol{q}$ represent a set of primitive variables to be defined in the following sections.

Remark 2. *Ideally, we would like to have a well-founded explicit choice of family of paths Ψ that satisfies (87). This is not trivial with our current approach. In particular, we are not aware of any proof that some path Ψ corresponding to any choice of $\boldsymbol{B}_{j+1/2}$ always exists. However, Proposition 6 guarantees that our schemes would be formally consistent with respect to any such implicitly defined path.*

Nevertheless, as the schemes we study may be trivially adapted to more formally derived cell-interface matrices $\boldsymbol{B}_{j+1/2}$, the simple averaging (118) seems adequate for heuristic purposes.

In particular, numerical tests indicate that schemes which are mutually *formally path-consistent* (more precisely, based on the same averaging of $\boldsymbol{B}_{j+1/2}$) converge to solutions that are identical to plotting accuracy, as is discussed in more detail in Sections 4.4 and 4.6.

3.3.1. *Six-equation system.* For the six-equation system, the canonical form (68) allows several choices for $\boldsymbol{q}$. Here we take

$$\boldsymbol{q} = \begin{bmatrix} \alpha_{\mathrm{g}} & p & v_{\mathrm{g}} & v_{\ell} & \rho_{\mathrm{g}} & \rho_{\ell} \end{bmatrix}^T \tag{119}$$

for simplicity. With the average $q_{i,j+1/2}$ from (118), all the remaining quantities in $\boldsymbol{B}_{j+1/2}$ can be calculated using the equation of state and constitutive relations.

3.3.2. *Four-equation system.* For the four-equation system, we use a reduced version of (119):

$$\boldsymbol{q} = \begin{bmatrix} \alpha_{\mathrm{g}} & p & v_{\mathrm{g}} & v_{\ell} \end{bmatrix}^T. \tag{120}$$

This yields

$$\boldsymbol{B}_{j+1/2} = \begin{bmatrix} 0 \\ 0 \\ \alpha_{\mathrm{g},j+1/2} \\ \alpha_{\ell,j+1/2} \end{bmatrix}. \tag{121}$$

3.4. **Second-order extension.** To obtain second-order spatial accuracy, we propose to use a semi-discrete version of the monotone upwind-centred scheme for conservation laws (MUSCL) [49, 30]. Herein, a piecewise linear function is constructed by using the data $\{\boldsymbol{u}_j(t)\}$. At each side of the interface $x_{j+1/2}$ we have values from the linear approximations in the neighbouring cells. These are denoted by

$$\boldsymbol{u}_j^{\mathrm{R}} = \boldsymbol{u}_j + \frac{\Delta x}{2}\boldsymbol{l}_j \quad \text{and} \quad \boldsymbol{u}_{j+1}^{\mathrm{L}} = \boldsymbol{u}_{j+1} - \frac{\Delta x}{2}\boldsymbol{l}_{j+1}, \tag{122}$$

where $\boldsymbol{l}_j$ are the slopes calculated using a suitable slope-limiter function.

There are several possible choices of variables to use in the slope-limiting procedure. The most accurate choice would be to use the characteristic variables. However, for the general two-fluid model, the characteristic variables are only available through a numerical diagonalization of the coefficient matrix of the equation system. Since one of the main advantages of the MUSTA scheme is its simplicity, we have chosen to employ the primitive variables $[\alpha_{\mathrm{g}}, p, v_{\mathrm{g}}, v_\ell, T_{\mathrm{g}}, T_\ell]$ instead. After this procedure, the flux $\boldsymbol{f}_{j+1/2}$ and the vector $\boldsymbol{w}_{j+1/2}$ are computed from $(\boldsymbol{u}_j^{\mathrm{R}}, \boldsymbol{u}_{j+1}^{\mathrm{L}})$, precisely as described in Section 3.2. That is, the linear reconstruction (122) *only* affects the Riemann problem (113) to be solved on the local grid. It should be noted that the cell-interface matrix is still a function of the non-reconstructed variables. That is, $(\boldsymbol{u}_j^{\mathrm{R}}, \boldsymbol{u}_{j+1}^{\mathrm{L}})$ are not involved in the evaluation of $\boldsymbol{B}_{j+1/2}$. Consequently, the properties p1 and p2 still hold.

For use with the MUSCL scheme, the system of balance equations (66) is semi-discretized:

$$\frac{\mathrm{d}\boldsymbol{u}_j}{\mathrm{d}t} + \frac{\boldsymbol{f}_{j+1/2} - \boldsymbol{f}_{j-1/2}}{\Delta x} + \frac{\boldsymbol{d}_{j-1/2}^+ + \boldsymbol{d}_{j+1/2}^-}{\Delta x} = \boldsymbol{s}_j, \tag{123}$$

where $\boldsymbol{d}_{j+1/2}^\pm$ are still defined by (90)–(91). To obtain a second-order solution in time, we employ the two-stage second-order strong-stability-preserving (SSP) Runge–Kutta (RK) method (see for instance [22]). With (123) of the form

$$\frac{\mathrm{d}\boldsymbol{u}_j}{\mathrm{d}t} = \mathcal{L}(\boldsymbol{u}_j), \tag{124}$$

the two-stage second-order SSP-RK scheme can be written as

$$\begin{aligned} \boldsymbol{u}_j^{(1)} &= \boldsymbol{u}^n + \Delta t\mathcal{L}(\boldsymbol{u}^n) \\ \boldsymbol{u}^{n+1} &= \frac{1}{2}\boldsymbol{u}^n + \frac{1}{2}\boldsymbol{u}^{(1)} + \frac{1}{2}\Delta t\mathcal{L}(\boldsymbol{u}^{(1)}). \end{aligned} \tag{125}$$

Herein, $\boldsymbol{u}_j^n$ is the vector of unknowns from time step n, $\boldsymbol{u}_j^{n+1}$ is the sought values at the next time step, while $\boldsymbol{u}_j^{(1)}$ represents intermediate values. In conjunction with the first-order MUSTA scheme, we perform the time stepping using the Forward Euler method.

4. Numerical simulations

In this section, the MUSTA scheme for the two-fluid model is analysed with respect to stability, accuracy and robustness using benchmark cases from the literature. Furthermore, it is compared to independent schemes, namely a Roe scheme for the four-equation model (Roe4) and the Rusanov scheme for the six-equation model.

The Roe4 is described in more detail in [16, 27]. It directly provides an upwind-type resolution of all waves. This makes it a suitable reference for the accuracy and efficiency of the MUSTA scheme, which attempts to obtain this upwind information numerically.

Furthermore, the Roe4 scheme is formally path-consistent with the MUSTA scheme, in the sense that the non-conservative integrals are identically evaluated. The path-consistency of the Roe4 scheme in this sense is discussed in [16], Section 3.2.

Comparisons with the Roe scheme are made for the four-equation model in Section 4.4.1. A Roe scheme is not yet available for the full two-fluid model in the canonical form of Section 2.3.3. Instead, the Rusanov scheme is used in Section 4.6 for comparing the converged solutions of the six-equation model. As the Rusanov scheme is highly diffusive for the slow waves, it is otherwise not suited as a benchmark for the performance of the MUSTA scheme.

Table 1: Equation-of-state parameters employed for the six-equation system.

	κ_k (−)	p_k^∞ (Pa)	$C_{p,k}$ (J/(kg K))
gas (g)	1.4	0.0	1008.7
liquid (ℓ)	2.8	8.5×10^8	4186.0

Table 2: Initial state for the moving-discontinuity problem.

Quantity	Symbol (unit)	Left	Right
Gas vol. frac.	α_g (−)	$1 - \varepsilon$	ε
Pressure	p (MPa)	0.1	0.1
Gas velocity	v_g (m/s)	100	100
Liq. velocity	v_ℓ (m/s)	100	100
Temperatures	$T_{g,\ell}$ (K)	315.9	315.9

4.1. **Thermodynamic submodels.** The analysis presented so far is independent of the equation of state, but to proceed with computations, a choice has to be made. For the calculations performed using the four-equation model described in Section 2.1, the following equation of state is employed:

$$p = c_k^2(\rho_k - \rho_k^\circ). \tag{126}$$

Herein, the speed of sound, c_k, and 'reference' density, ρ_k°, are constants for each phase k. In the following calculations, we have adapted the parameters c_k and ρ_k° in each case, to produce results comparable to those of the six-equation model. Given the composite variables $[(\alpha\rho)_g, (\alpha\rho)_\ell, (\alpha\rho v)_g, (\alpha\rho v)_\ell]$, one can calculate the primitive variables $[\alpha_g, p, v_g, v_\ell]$ after employing a quadratic equation for the pressure. This equation is found by writing (126) for each phase while noting the equality of pressure in the two phases and using the relation $\alpha_g + \alpha_\ell = 1$.

The equation of state that has been used for the six-equation model (see Section 2.2) is

$$p = (\kappa_k - 1)\rho_k e_k - \kappa_k p_k^\infty, \tag{127}$$

where the ratio of specific heats, κ_k, and the 'reference' pressure, p_k^∞, are constants for each phase. This stiffened-gas equation of state is common in the literature [31, 6, 9]. For all the presented six-equation calculations, we have used the parameters given in Table 1 to facilitate comparison with results from the literature [31]. With the composite variables $[(\alpha\rho)_g, (\alpha\rho)_\ell, (\alpha\rho v)_g, (\alpha\rho v)_\ell, E_g, E_\ell]$ one can calculate the primitive variables $[\alpha_g, p, v_g, v_\ell, T_g, T_\ell]$ similarly to what is done in the four-equation case. Herein, the temperature is found as

$$T_k = \frac{e_k - p_k^\infty/\rho_k}{C_{v,k}}. \tag{128}$$

Further details are given by Paillère *et al.* [31].

We are now equipped to perform numerical calculations, which is the theme of the following sections. Results labelled 'MUSCL-MUSTA' have been calculated using the second-order scheme, whereas the first-order scheme has been used for the results labelled 'MUSTA'. The numbers 4 or 6 will be appended to the scheme names to indicate whether they are for the four-equation or six-equation system. For the calculations, $M = 4$ stages and $2N = 4$ local cells have been chosen as a default in the MUSTA procedure, since this seems to be a reasonable compromise between accuracy and speed. Other choices are sometimes preferable, and this will be indicated.

4.2. **Moving discontinuity.** It is a basic test for numerical schemes that when no source terms are present, a flow with a uniform velocity and pressure should remain so, that is, variations should not be introduced in the velocities or in the pressure. This has sometimes been referred to as the principle of Abgrall [1].

The agreement with Abgrall's principle was checked by performing a calculation in a 12 m long horizontal tube, where the initial state consists of uniform velocities, temperatures and pressure, but where there is a jump in the volume fraction, see Table 2. At the middle of the tube, the gas volume fraction jumps from $1 - \varepsilon$ to ε, where $\varepsilon = 1 \times 10^{-12}$. This gives practically single-phase flow on each side of the discontinuity. A similar case was considered in [9]. The six-equation model was employed, and the equation-of-state parameters are those given in Table 1.

The results at time $t = 0.03$ s displayed in Figure 2 have been calculated using the MUSCL-MUSTA6$_{4-4}$ scheme (four local steps and four local cells) with the van Leer [47] slope on a 200-cell

(a) Gas volume fraction   (b) Pressure
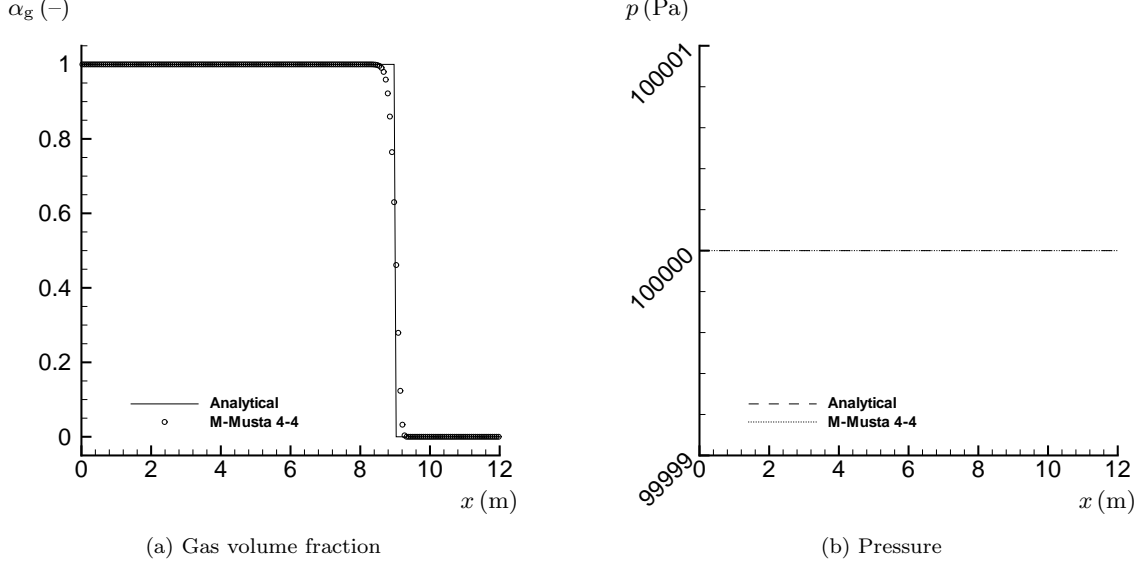
Figure 2: Moving discontinuity (six-equation system). MUSCL-MUSTA6$_{4-4}$ using the van Leer slope, 200 cells, $r = 0.5$.

grid. The CFL number was $r = 0.5$. Ideally, the volume fraction should be advected, but not smeared. As shown in Figure 2(a), some smearing takes place, but the volume fraction is relatively sharply resolved. Figure 2(b) demonstrates that no significant disturbances are introduced in the pressure. Let us define the maximum relative pressure disturbance for the calculation as

$$\mathscr{E}_p = \frac{1}{p^0} \max_{\forall n} \big\{ |\max_{\forall j} p_j^n - \min_{\forall j} p_j^n| \big\}, \tag{129}$$

where p^0 is the initial pressure, j is the spatial index and superscript n denotes the time step. Here, $\mathscr{E}_p \approx 4 \times 10^{-11}$, which is in the range of the round-off error. For calculations performed with double double precision, $\mathscr{E}_p$ was reduced by 18 orders of magnitude. Hence it is possible that $\mathscr{E}_p = 0$ in exact arithmetics. An interesting direction for further research would be to check this analytically.

It should be said that numerical instabilities caused the Roe4 scheme to fail on this case with such a low value for ε.

4.3. **Moving Gauss curve.** This case has been designed to test the convergence order of the schemes for smooth solutions. It is identical to the moving-discontinuity case, except for the initial value of the gas volume fraction, which is a scaled Gauss curve:

$$\alpha_{\mathrm{g},0} = (1 - 2\varepsilon) \exp\left(-\frac{(x - \mu)^2}{2\sigma^2} \right) + \varepsilon, \tag{130}$$

where $\sigma = 0.42\,\mathrm{m}$, $\mu = 6\,\mathrm{m}$, and where $\varepsilon = 1 \times 10^{-12}$ is the same as for the moving-discontinuity case.

Calculations have been performed with periodic boundary conditions until $t = 0.03\,\mathrm{s}$, so that the exact solution is the same curve, centred at $x = 9\,\mathrm{m}$, see Figure 3. It can be observed that there is an asymmetry in the data about the line $x = 9\,\mathrm{m}$. This is a property of the slope limiter.

The error in the calculated gas volume fractions at a given time step has been quantified using the 1-norm:

$$\|\mathscr{E}(\alpha_{\mathrm{g}})\|_1 = \Delta x \sum_{\forall j} |\alpha_{\mathrm{g},j} - \alpha_{\mathrm{g,ref},j}|, \tag{131}$$

where the subscript 'ref' indicates the reference solution, which is the exact solution in this case.
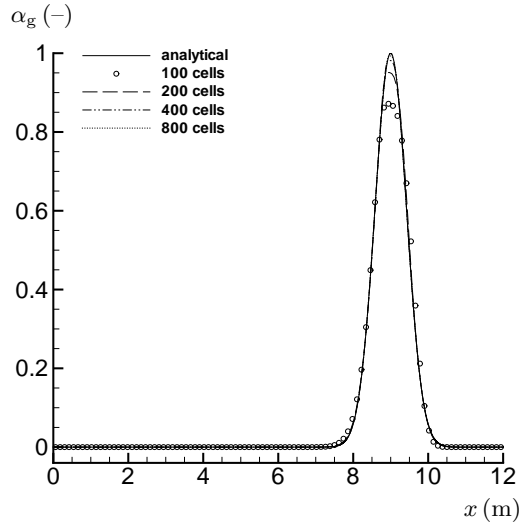
Figure 3: Moving Gauss curve (six-equation system). Grid refinement for MUSCL-MUSTA6$_{4-4}$ using the van Leer slope. $r = 0.5$.

Table 3: Moving Gauss curve. Convergence order, n, and 1-norm of the error in the gas volume fraction by grid refinement.

Δx(m)	MUSTA6$_{4-4}$		MUSCL-MUSTA6$_{4-4}$	
	$\|\mathscr{E}(\alpha_\mathrm{g})\|_1$	n	$\|\mathscr{E}(\alpha_\mathrm{g})\|_1$	n
0.015	1.195×10^{-1}	–	2.222×10^{-3}	–
0.0075	6.328×10^{-2}	0.92	5.557×10^{-4}	2.00
0.00375	3.263×10^{-2}	0.96	1.375×10^{-4}	2.01
0.001875	1.658×10^{-2}	0.98	3.398×10^{-5}	2.02
0.0009375	8.356×10^{-3}	0.99	8.364×10^{-6}	2.02

Table 3 shows the convergence order and 1-norm of the error for MUSTA6$_{4-4}$ and MUSCL-MUSTA6$_{4-4}$. The former scheme was run with a CFL number of $r = 0.9$ and the latter with $r = 0.5$. As can be seen, the attained convergence order is as expected: MUSTA6 is first order, while MUSCL-MUSTA6 is second order.

4.4. **Water faucet.** The water-faucet test case introduced by Ransom [34] constitutes a standard test for one-dimensional two-fluid models and methods for their numerical resolution. It has been studied for instance in [11, 46, 16, 31, 27].

Initially, the state in the water faucet is uniform. The values are given in Table 4. The inlet boundary conditions are equal to the initial values for the gas volume fraction, and the gas and liquid velocities. A pressure equal to the initial pressure is specified at the outlet. At time $t = 0$, gravity ($g = 9.81 \, \mathrm{m/s}^2$) is turned on, and the liquid column starts thinning as a discontinuity moves towards the exit. In the following, the results are given at $t = 0.6 \, \mathrm{s}$. An approximate analytical solution is available, and it can be found for instance in [16].

4.4.1. *Four-equation system.* We first consider the MUSTA4 scheme for the four-equation system. The employed equation-of-state parameters are shown in Table 5. Note that they are different from the values previously used in [16, 27]. The modifications have been performed to obtain similar speeds of sound to those produced by the six-equation system with common parameter values for the stiffened-gas equation of state [31].

Table 4: Initial state in the water-faucet test problem.

Quantity	Symbol (unit)	Value
Gas vol. frac.	α_g (−)	0.2
Pressure	p (MPa)	0.1
Gas velocity	v_g (m/s)	0.0
Liquid velocity	v_ℓ (m/s)	10.0

Table 5: Parameters employed in the water-faucet test problem (four-equation system).

	c_k (m/s)	ρ_k° (kg/m^3)
gas (g)	357.014	0.313824
liquid (ℓ)	1542.80	999.978
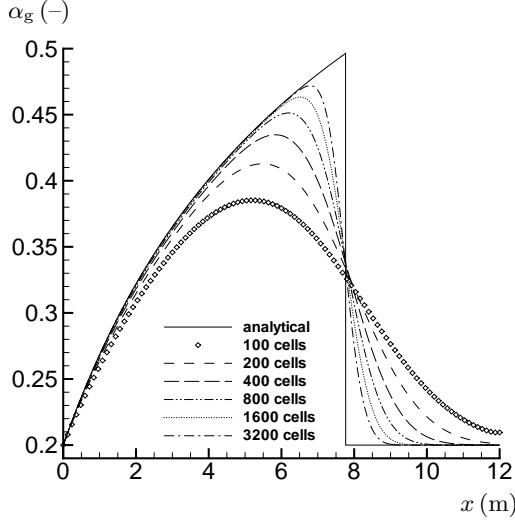
(a) Grid refinement for MUSTA4$_{4-4}$
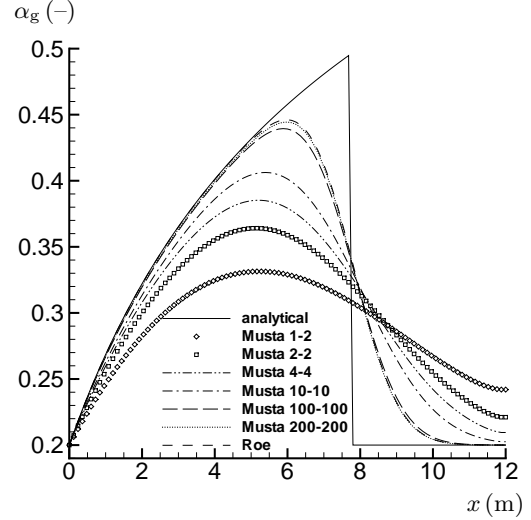
(b) Varying number of stages and local cells in MUSTA4$_{M-2N}$. 100 'global' cells.

Figure 4: Volume fraction for the water faucet (four-equation system). Influence of grid, number of stages, and number of local cells in the MUSTA4 scheme. $r = 0.9$.

Figure 4(a) shows the gas volume fraction calculated using the MUSTA4$_{4-4}$ scheme and a constant CFL number of $r = 0.9$. As the grid is refined, the solution converges steadily, but slowly.

An important difference between MUSTA4 and Roe4 is illustrated in Figure 4(b), which shows the effect of increasing the number of local time steps (M) and local cells ($2N$) in the MUSTA4$_{M-2N}$ scheme. A 100-cell grid and $r = 0.9$ was used. MUSTA4$_{1-2}$ is similar to FORCE and is, as expected, quite diffusive. However, MUSTA4 needed as much as 200 local time steps and 200 local cells to produce a volume-fraction profile comparable to that obtained using the Roe4 scheme.

The faucet case has also been calculated with the MUSCL-MUSTA4$_{4-4}$ scheme. Different slope-limiter functions were tested, namely the superbee and the minmod slope (see [25], Section 9.2), the van Leer [47] slope (see also [48]) and the monotonized central-difference (MC) slope [48]. The latter three slopes gave acceptable results, whereas the superbee slope gave oscillations. The MC slope gave the best results in this case, and they are displayed in Figure 5. The CFL number was $r = 0.5$.

The volume-fraction profiles of MUSCL-MUSTA4$_{4-4}$ in Figure 5(a) can be compared to those of the first-order MUSTA4$_{4-4}$ scheme in Figure 4(a), and it can be seen that the MUSCL approach constitutes an improvement. However, the results are not quite as good as those obtained using the Roe4 scheme [27] with characteristic flux-limiting. The remaining physical variables are displayed

(a) Gas volume fraction

(b) Pressure

(c) Gas velocity

(d) Liquid velocity
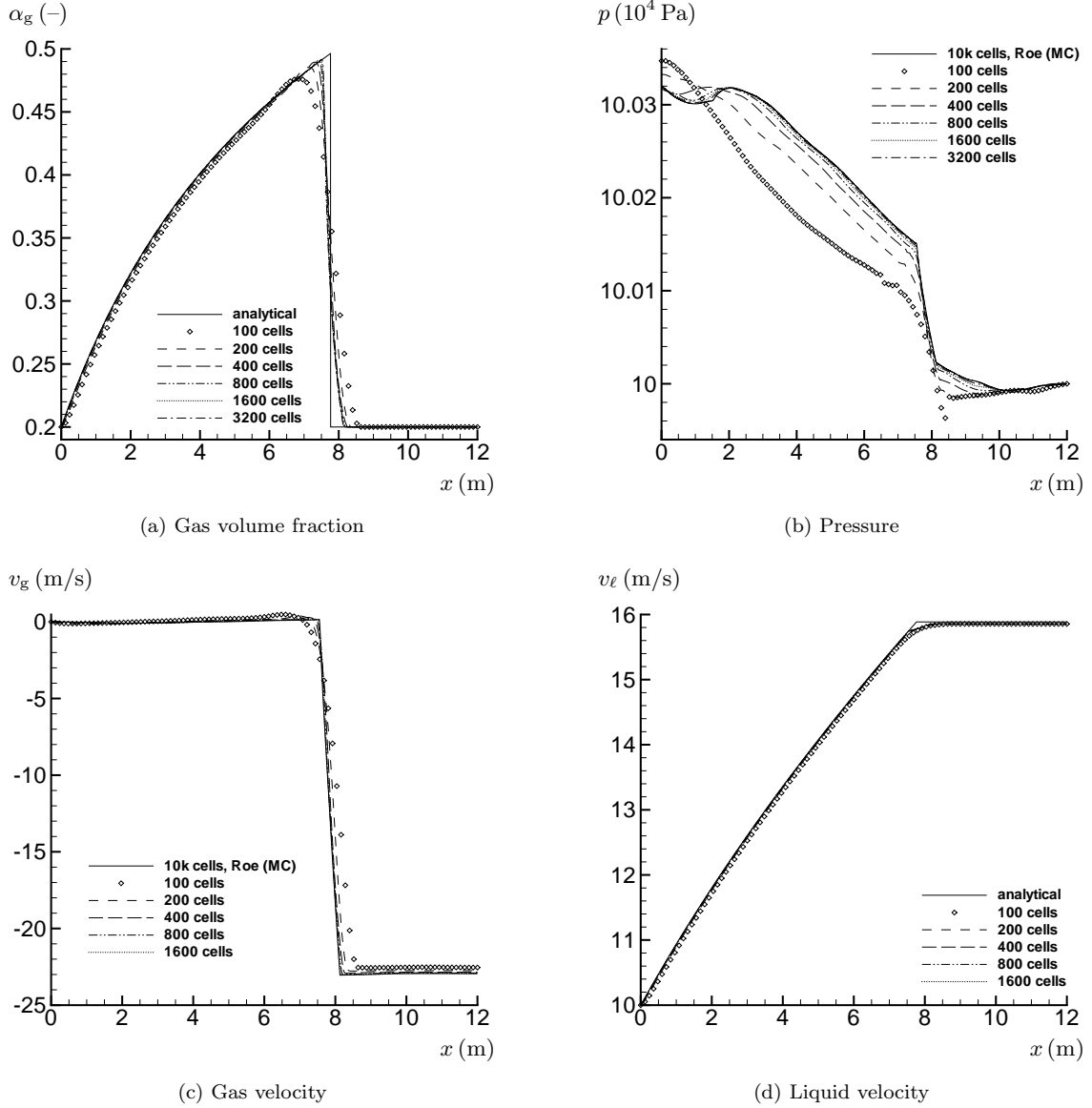
Figure 5: Water faucet (four-equation system). Convergence of the MUSCL-MUSTA4$_{4-4}$ scheme using the MC slope. $r = 0.5$.

in Figures 5(b)–5(d). Data obtained using the Roe4 scheme with the MC flux limiter on a 10000-cell grid are given as reference solutions for the gas velocity and for the pressure, where an analytical solution is not available. The velocities are accurately represented even on relatively coarse grids, while finer grids are needed to resolve the pressure (see Figure 5(b)).

Figure 6 illustrates the efficiency of MUSTA4$_{M-2N}$ and MUSCL-MUSTA4$_{M-2N}$ for different combinations of M and $2N$. The ordinate is the 1-norm (131) of the gas volume fraction, where the reference solution is that obtained using the MC-limited Roe4 scheme on a 10000-cell grid. The abscissa is the CPU time non-dimensionalized with the CPU-time of the Roe4 (MC) scheme on a 100-cell grid. The calculations have been performed with the same settings as those explained previously for the faucet case. In the figure, the rings (○) denote the results from the second-order versions of the schemes. It can be seen that for the faucet case, MUSCL-MUSTA4$_{2-2}$ is the

$\|\mathscr{E}(\alpha_\mathrm{g})\|_1 \, (-)$
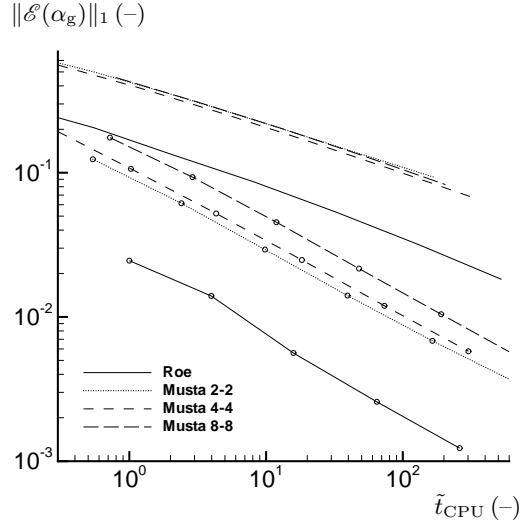
Figure 6: Water faucet (four-equation system). 1-norm of the error in the gas volume fraction as a function of non-dimensional CPU time, for different MUSTA4$_{M-2N}$ (without ∘) and MUSCL-MUSTA4$_{M-2N}$ schemes (with ∘). Results for the corresponding Roe4 schemes are also shown.

most efficient of the MUSTA schemes. The difference between the first-order MUSTA schemes are small, but MUSTA4$_{4-4}$ seems to be optimal. Further, it is evident that the MUSTA schemes are less efficient for the faucet case than their Roe counterparts. For a given accuracy, Roe4 needs roughly 5 % of the CPU time of MUSTA4$_{4-4}$, whereas (for a higher accuracy), Roe4 (MC) needs about 6–8 % of the CPU time of MUSCL-MUSTA4$_{2-2}$. It should be noted that the CPU time also depends on the specific implementation, so it must be understood that Figure 6 cannot be interpreted absolutely. We do, however, believe that our implementation of the schemes is sufficiently close to optimal that Figure 6 constitutes a fair comparison.

4.4.2. *Six-equation system.* We now turn to the MUSTA6 scheme for the six-equation system. The parameters employed in the equation of state (127) are given in Table 1, and the initial conditions are still the same as those of Table 4. However, additional conditions are needed due to the energy equation. Here we set the initial gas and liquid temperatures to $T_{\mathrm{g},0} = T_{\ell,0} = 315.9\,\mathrm{K}$. This value was chosen to obtain a liquid density of $\rho_{\ell,0} = 1000.0\,\mathrm{kg/m^3}$.

The boundary conditions were also the same as those in the four-equation case, but in addition, the entropy $s_\ell = s_\ell(p_0, \rho_{\ell,0})$ was used at the left-hand side boundary and $s_\mathrm{g} = s_\mathrm{g}(p_0, \rho_{\mathrm{g},0})$ was set at the right-hand side boundary. Herein,

$$s_k = C_{v,k} \ln\left(\frac{p_k + p_k^\infty}{\rho_k^\kappa} \right). \tag{132}$$

Figure 7 displays the physical variables obtained using the MUSCL-MUSTA6$_{4-4}$ scheme with the MC slope while refining the grid and keeping the CFL number at $r = 0.5$. The volume fraction, pressure and velocities in Figures 7(a)–7(d) are practically equal to those obtained with the four-equation model in Figures 5(a)–5(d), whereas, of course, the temperatures in Figures 7(e)–7(f) have no counterparts in the four-equation model. One can observe that the variation in liquid temperature is minuscule. The quantity plotted in Figure 7(f) is the final temperature subtracted by the initial temperature $T_{\ell,0} = 315.9\,\mathrm{K}$.
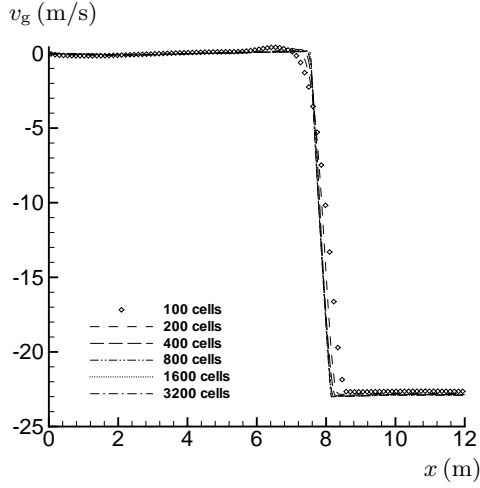
4.5. **Toumi's shock tube.** The present problem was introduced by Toumi [44] and it has been studied e.g. by [37, 31, 17]. It consists of a tube divided by a membrane in the middle. At $t = 0$, the membrane ruptures, and the flow starts evolving. The initial conditions are displayed in Table 6
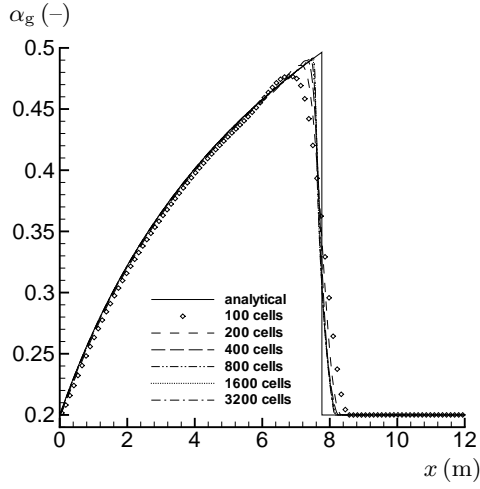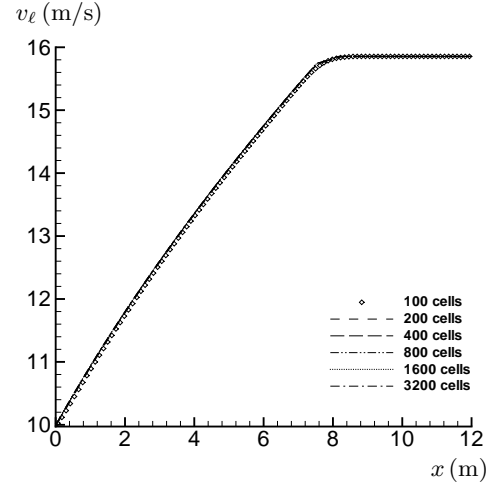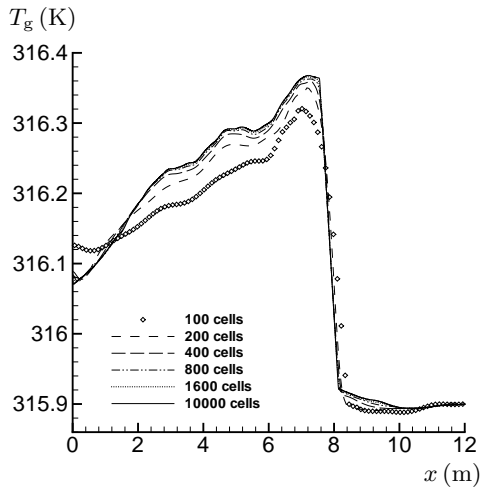
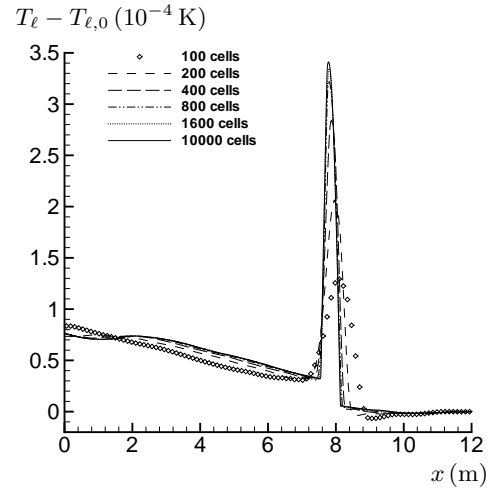(a) Gas volume fraction
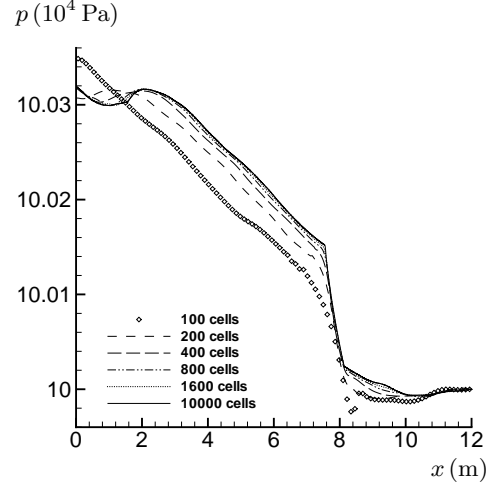
(b) Pressure

(c) Gas velocity

(d) Liquid velocity

(e) Gas temperature

(f) Liquid temperature

Figure 7: Water faucet (six-equation system). Convergence of the MUSCL-MUSTA6$_{4-4}$ scheme using the MC slope. $r = 0.5$.

Table 6: Initial state in Toumi's shock tube.

Quantity	Symbol (unit)	Left	Right
Gas vol. frac.	$\alpha_{\mathrm{g}}\,(-)$	0.25	0.10
Pressure	$p\,(\mathrm{MPa})$	20	10
Gas velocity	$v_{\mathrm{g}}\,(\mathrm{m/s})$	0	0
Liquid velocity	$v_{\ell}\,(\mathrm{m/s})$	0	0
Temperatures	$T_{\mathrm{g},\ell}\,(\mathrm{K})$	308.15	308.15

Table 7: Toumi's shock tube. MUSCL-MUSTA6$_{4-4}$ scheme. Convergence order, n, and 1-norm of the error in the gas volume fraction by grid refinement.

$\Delta x(\mathrm{m})$	$\|\mathscr{E}(\alpha_{\mathrm{g}})\|_1$	n
1.0	1.630×10^{-1}	–
0.5	1.204×10^{-1}	0.44
0.25	6.940×10^{-2}	0.79
0.1667	4.773×10^{-2}	0.92
0.125	3.473×10^{-2}	1.1
0.1	2.788×10^{-2}	0.98

and the employed equation-of-state parameters are given in Table 1. Following [31, 17] we took $\delta = 2$ in Equation (62). No source terms were considered.

The problem was analysed with the full six-equation model. Figure 8 shows the convergence of the four-step four-cell MUSCL-MUSTA6$_{4-4}$ scheme using the van Leer slope and a CFL number of $r = 0.5$. The results are for the time $t = 0.06\,\mathrm{s}$. As can be seen, the curves in Figure 8 are non-oscillatory. The error and convergence order based on the 1-norm of the volume fraction are reported in Table 7, where the numerical solution on a 10000-cell grid is used as reference. The convergence is of less than second order due to the discontinuities present in the solution. The present plots can be compared with those in [31], and they seem to converge towards highly similar solutions. However, particularly the shocks and the rarefactions are more sharply resolved in the present case.

4.6. **Effect of integration path.** In this section, we numerically investigate the sensitivity of the numerical solution to the choice of averaging method of the cell-interface matrix $\boldsymbol{B}_{j+1/2}$ described in Section 3.3, and thus implicitly the family of integration paths Ψ as described by Proposition 6. The test case is still Toumi's shock tube described in Section 4.5.

In the context of (116)–(118), we here consider three different ways of calculating the cell-interface matrix $\boldsymbol{B}_{j+1/2}$. In particular, with

$$\boldsymbol{B}_{j+1/2} = \boldsymbol{B}(\boldsymbol{u}(\boldsymbol{q}_{j+1/2})), \tag{133}$$

we consider the choices:

$$\boldsymbol{q}_{j+1/2} = \boldsymbol{q}_j \tag{134}$$

$$\boldsymbol{q}_{j+1/2} = \boldsymbol{q}_{j+1} \tag{135}$$

$$\boldsymbol{q}_{j+1/2} = \frac{1}{2}\left(\boldsymbol{q}_j + \boldsymbol{q}_{j+1}\right). \tag{136}$$

These will be denoted as the *left*, *right* and *arithmetic* averages, respectively.

Remark 3. *Note that (134) corresponds to the limit $\varepsilon \to 0$ for the family of paths given by*

$$\Psi(s; \boldsymbol{u}_j, \boldsymbol{u}_{j+1}) = \left\{ \begin{array}{ll} \boldsymbol{u}_j & \text{for} \quad s \leq 1 - \varepsilon \\ \boldsymbol{u}_j + (\boldsymbol{u}_{j+1} - \boldsymbol{u}_j)\frac{s+\varepsilon-1}{\varepsilon} & \text{for} \quad s > 1 - \varepsilon \end{array} \right. , \tag{137}$$

(a) Gas volume fraction

(b) Pressure

(c) Gas velocity

(d) Liquid velocity

(e) Gas temperature
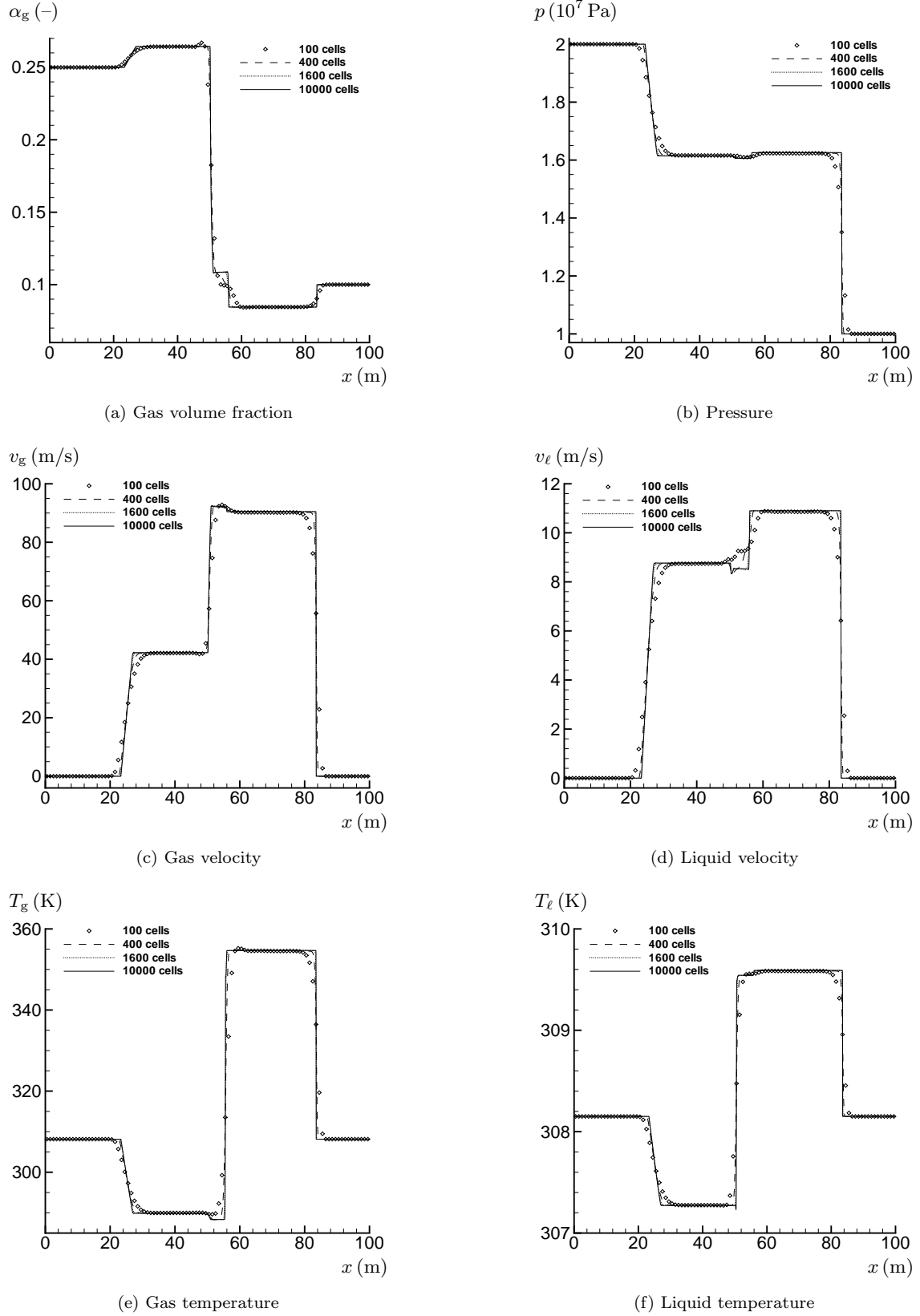
(f) Liquid temperature

Figure 8: Toumi's shock tube (six-equation system). Convergence of the MUSCL-MUSTA6$_{4-4}$ scheme using the van Leer slope. $r = 0.5$.

whereas (135) corresponds to the limit $\varepsilon \to 0$ for the family of paths given by

$$\Psi(s; \boldsymbol{u}_j, \boldsymbol{u}_{j+1}) = \begin{cases} \boldsymbol{u}_j + (\boldsymbol{u}_{j+1} - \boldsymbol{u}_j)\frac{s}{\varepsilon} & for \quad s \le \varepsilon \\ \boldsymbol{u}_{j+1} & for \quad s > \varepsilon \end{cases}. \tag{138}$$

Hence these may be interpreted as the extremal left-biased and right-biased paths, respectively.

To evaluate the above-mentioned averages in the MUSTA scheme, we employ the Rusanov scheme as reference. In the Rusanov scheme, the arithmetic average (136) is employed. In particular, the scheme will be *formally consistent* with respect to any family of paths implicitly defined by this average. Based on the results in [7], we expect the MUSTA scheme based on the arithmetic average (136) to converge to solutions highly similar to those of the Rusanov scheme, whereas the extreme left and right-biased averages (134) and (135) are expected to yield different solutions.

Figure 9 shows the physical variables calculated with the MUSCL-MUSTA6$_{4-4}$ scheme using the van Leer slope and a CFL number of $r = 0.5$ on a fine grid of 10000 cells. The data are plotted for $t = 0.06$ s. The reference is obtained using the Rusanov scheme with a CFL number of $r = 0.9$ and a very fine grid of 320000 cells. The figure indicates that to plotting accuracy, MUSTA with arithmetic averaging and Rusanov converge to the same solution for all the variables. On the other hand, using different averages for $\boldsymbol{q}_{j+1/2}$ in MUSTA results in different levels of two of the plateaux, see for instance Figure 9(c).

It should be noted that since we cannot prove that our schemes converge uniformly in the sense of graphs, we do not know if the converged solutions are really identical or only near-identical. In fact, the latter may very well be most likely; see [7] for details. Any such difference between the converged solutions would only clearly appear on much finer grids than the ones considered here.

On the other hand, our results clearly illustrate how different choices of families of paths may lead to different converged numerical solutions.

4.7. **Water-air separation.** The water-air separation problem was introduced by Coquel *et al.* [11] and has been studied in, among others, [16, 31, 18]. It consists of a vertical tube of length $L = 7.5$ m, closed at both ends. Initially it has a uniform pressure of $p = 1 \times 10^5$ Pa, a volume fraction of $\alpha_\ell = 0.5$ and a temperature of $T = 315.9$ K. At time $t = 0$, the phases start separating under the influence of gravity.

In a frictionless model, the gas velocity may attain very large values at the end of the tube, where the gas is disappearing. Similar problems were observed by Evje and Flåtten [18], who included an interfacial drag term in the governing equations:

$$\tau_F = F\alpha_g\alpha_\ell\rho_g(v_g - v_\ell). \tag{139}$$

Herein, the friction parameter F is positive. A similar formulation was also used by Paillère *et al.* [31]. To limit the interfacial friction to the near-single-phase liquid regions, we employ a friction parameter similar to the one of Evje and Flåtten [18]:

$$F = k_1 e^{-k_2 \alpha_g}, \tag{140}$$

where $k_1 = 5 \times 10^4$ s^{-1} and $k_2 = 50$.

The water-air separation problem poses a great challenge regarding the robustness of the scheme. Even with the above interfacial friction model, the gas velocity develops a peak which can spur instabilities. Further challenges include steep gradients combined with the volume fractions approaching 0 and 1. Notably, the Roe scheme is not robust enough to be used for this problem.

We employ the six-equation system and the MUSTA6$_{2-2}$ scheme with a CFL number of $r = 0.3$. The choice $M = 2$, $2N = 2$ has been made to obtain a high degree of robustness in the MUSTA procedure. Figure 10 shows data plotted at $t = 0.6$ s, that is, before a steady state is reached. The analytical reference solutions are approximate (more so than the ones for the faucet case), and can be found in [16]. Even so, they agree well with the converged solutions. For a given grid, the present method does not resolve the discontinuities particularly sharply, but it is robust and not prone to numerical oscillations. The convergence order of the scheme is reported in Table 8, where the approximate analytical solution is used as reference.
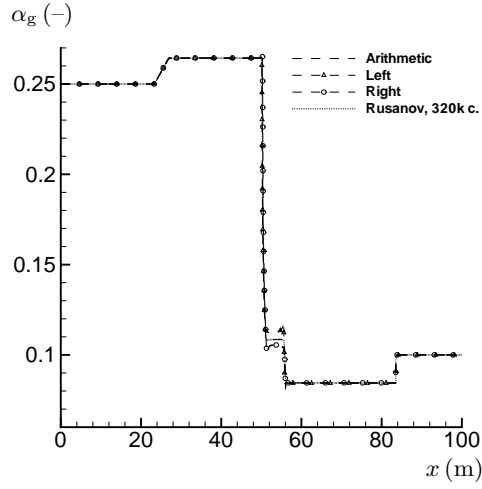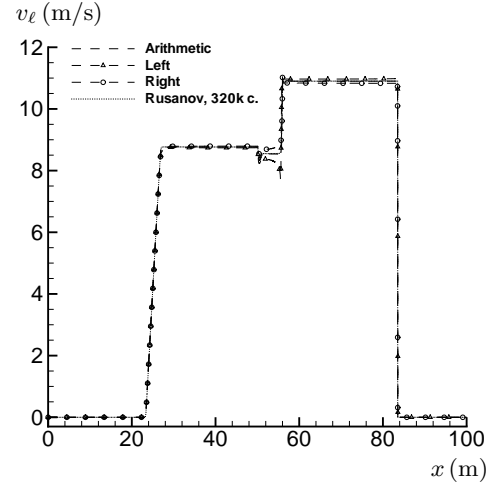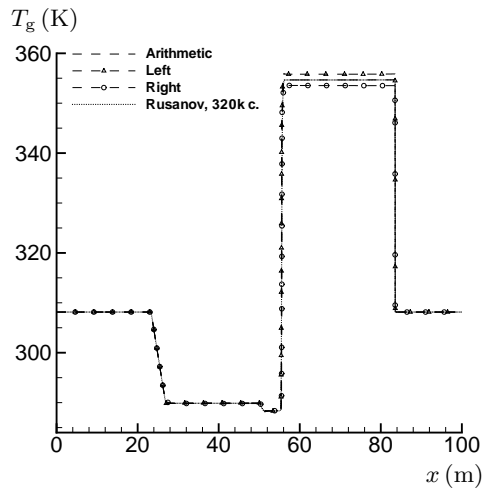
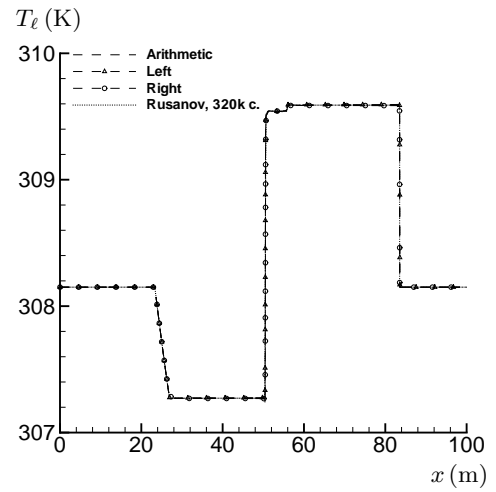(a) Gas volume fraction
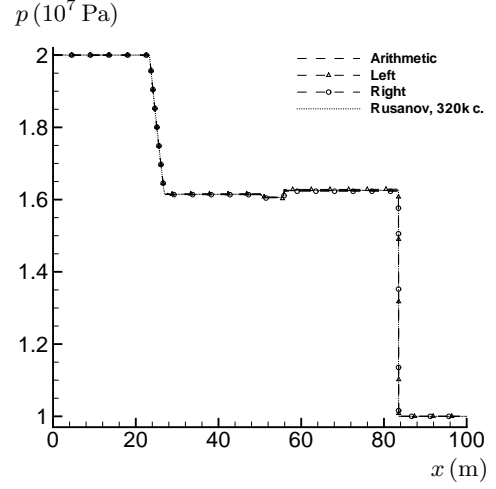
(b) Pressure
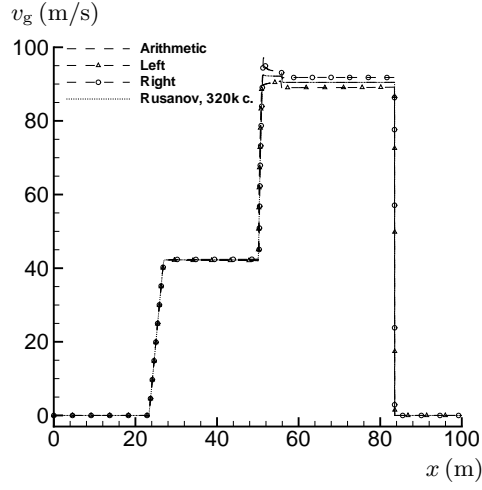
(c) Gas velocity

(d) Liquid velocity

(e) Gas temperature

(f) Liquid temperature

Figure 9: Toumi's shock tube (six-equation system). Effect of averaging method for $\boldsymbol{q}_{j+1/2}$. MUSCL-MUSTA6$_{4-4}$, 10000 cells, $r = 0.5$.
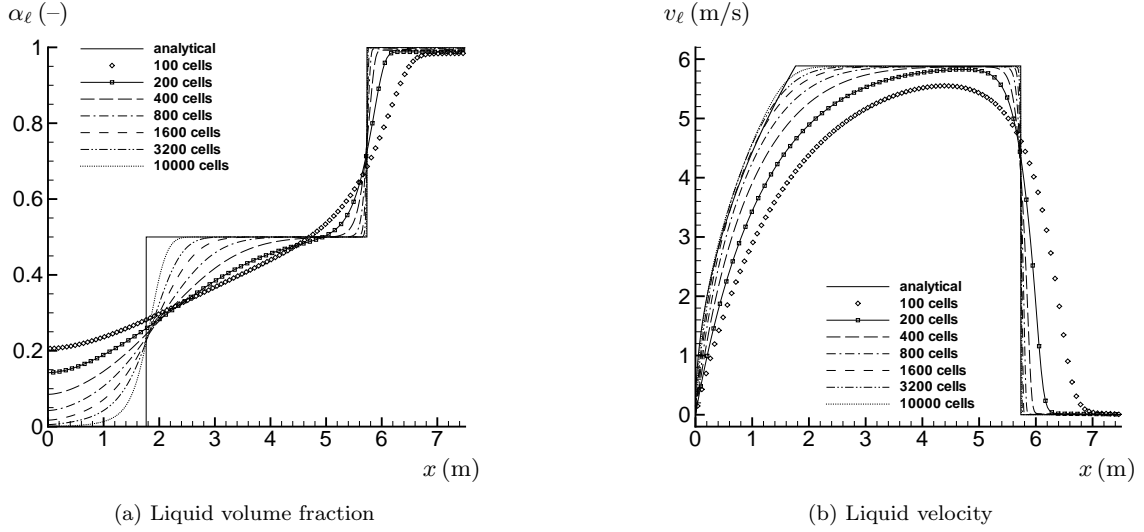
(a) Liquid volume fraction   (b) Liquid velocity

Figure 10: Water–air separation at $t = 0.6\,\mathrm{s}$ (six-equation system). Convergence of the MUSTA6$_{2-2}$ scheme. $r = 0.3$.

Table 8: Water-air separation, $t = 0.6\,\mathrm{s}$. MUSTA6$_{2-2}$ scheme. Convergence order, n, and 1-norm of the error in the gas volume fraction by grid refinement.

$\Delta x(\mathrm{m})$	$\|\mathscr{E}(\alpha_\mathrm{g})\|_1$	n
0.075	9.931×10^{-1}	–
0.0375	7.685×10^{-1}	0.37
0.01875	5.747×10^{-1}	0.42
0.009375	4.184×10^{-1}	0.46
0.0046875	3.008×10^{-1}	0.48

Data for $t = 1.5\,\mathrm{s}$, that is, when a steady state has ideally been reached, are displayed in Figure 11. For fine grids, the expected sharp volume-fraction profile is attained (Figure 11(a)), and likewise for the hydrostatic pressure profile (Figure 11(b)). The physical interpretation of the calculated velocity profiles is not obvious, since the velocity is non-zero mainly where the corresponding phase is practically absent (Figures 11(c) and 11(d)). A similar comment holds for the gas temperature (Figure 11(e)). As for for the liquid, the calculated temperature variations shown in Figure 11(f) are in the order of milli-Kelvin.

Figure 11(c) shows that the interfacial friction model has succeeded reasonably well in limiting the gas velocity. One exception is at the interface, that is, where the volume fraction varies strongly. There, the gas is still present, but the interfacial friction is low due to the exponential term in the equation (140).

5. Summary

Some steps towards a more formal numerical treatment of non-conservative terms in a two-phase pipe flow model have been made. In particular, we have presented a mathematical transformation eliminating non-conservative time derivatives from a common six-equation model containing energy transfers. Furthermore, we have shown how *formally path-consistent* numerical schemes may be constructed for this model.

Our numerical experiments verify that numerical schemes which are not formally consistent with respect to the same family of paths will converge to different weak solutions. On the other
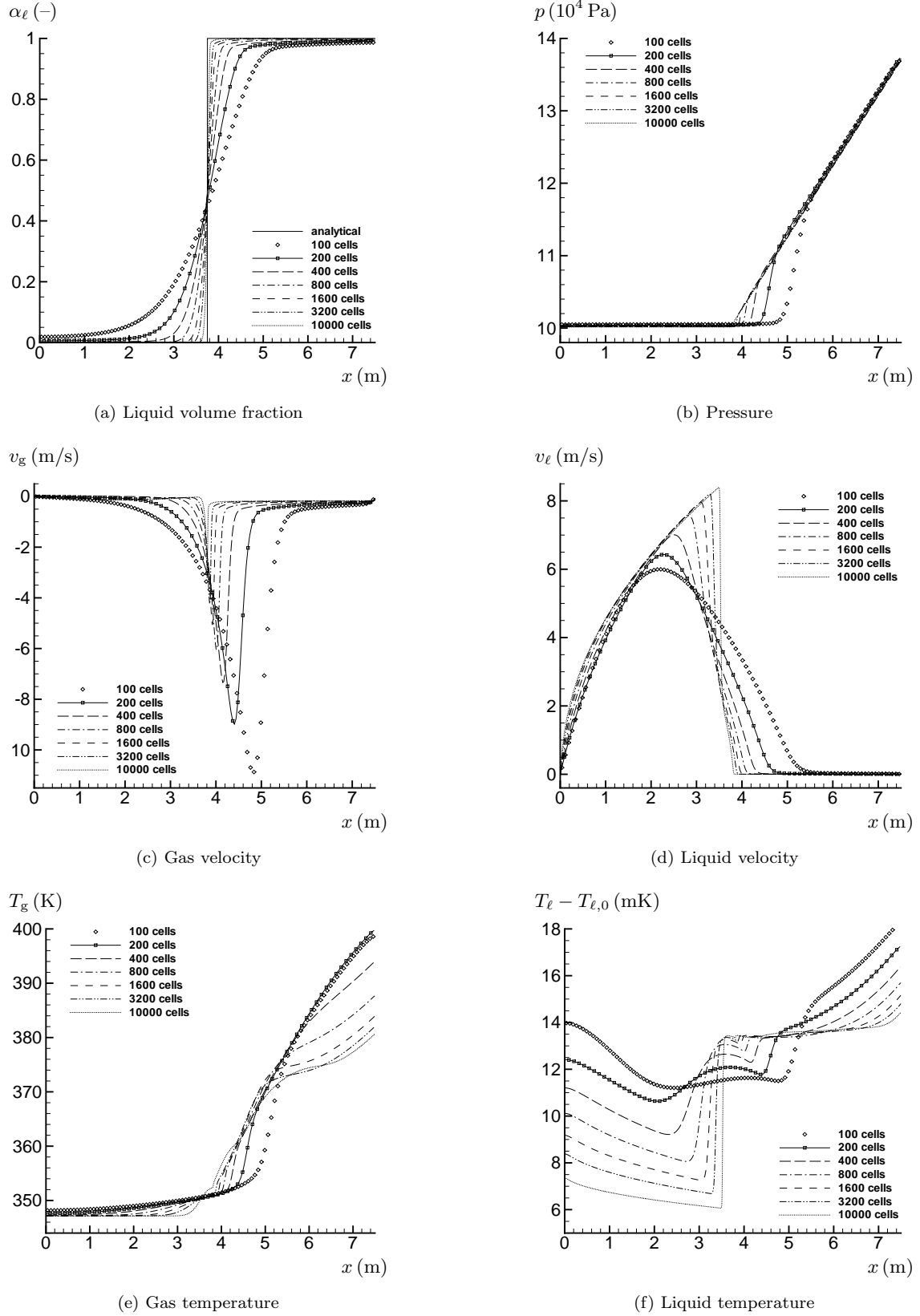
(a) Liquid volume fraction

(b) Pressure

(c) Gas velocity

(d) Liquid velocity

(e) Gas temperature

(f) Liquid temperature

Figure 11: Water–air separation at $t = 1.5\,\text{s}$ (six-equation system). Convergence of the MUSTA6$_{2-2}$ scheme. $r = 0.3$.

hand, schemes that *are* mutually formally path-consistent (in the weaker sense made precise in Section 3.3) yield solutions that are close to identical; any discrepancies between the converged solutions do not emerge even for relatively fine grids. This is consistent with the results proved in [7].

Specifically, we have proposed a MUSTA multi-stage central-type scheme for our non-conservative two-fluid model. The MUSTA scheme has been compared to a Roe scheme for the four-equation model. In general, MUSTA did not achieve the same accuracy and efficiency as Roe on moving-discontinuity problems such as the water-faucet case. On the other hand, the MUSTA scheme was robust enough to handle such cases as water-air separation, where the Roe scheme failed. On a wide range of problems, the MUSTA scheme produced accurate and non-oscillatory results. This, combined with its generality and relative ease of implementation, is its strength.

References

[1] R. Abgrall, How to prevent pressure oscillations in multicomponent flow calculations: A quasi conservative approach, *J. Comput. Phys.* **125**, 150–160, (1996).

[2] K. H. Bendiksen, D. Malnes, R. Moe, and S. Nuland, The dynamic two-fluid model OLGA: Theory and application, in *SPE Prod. Eng.* **6**, 171–180, (1991).

[3] A. Bermudez and M. E. Vazquez, Upwind methods for hyperbolic conservation laws with source terms, *Comput. Fluids* **23**, 1049–1071, (1994).

[4] D. Bestion, The physical closure laws in the CATHARE code, *Nucl. Eng. Des.* **124**, 229–245, (1990).

[5] S. Bianchini and A. Bressan, Vanishing viscosity solutions of nonlinear hyperbolic systems, *Ann. of Math.* **161**, 223–342, (2005).

[6] C. E. Castro and E. F. Toro, A Riemann solver and upwind methods for a two-phase flow model in non-conservative form, *Int. J. Numer. Meth. Fl.* **50**, 275–307, (2006).

[7] M. J. Castro, P. G. LeFloch, M. L. Muñoz-Ruiz and C. Parés, Why many theories of shock waves are necessary: Convergence error in formally path-consistent schemes, *J. Comput. Phys.* **227**, 8107–8129, (2008).

[8] M. J. Castro, C. Parés, A. Pardo and E. F. Toro, Well-balanced high-order MUSTA schemes for non-conservative hyperbolic systems, in *Numerical Mathematics and Advanced Applications*, Proceedings of ENU-MATH 2007, the 7th European Conference on Numerical Mathematics and Advanced Applications, Graz, Austria, September 2007, Springer Berlin Heidelberg, Germany (2008).

[9] C.-H. Chang and M.-S. Liou, A robust and accurate approach to computing compressible multiphase flow: Stratified flow model and AUSM$^+$-up scheme, *J. Comput. Phys.* **225**, 850–873, 2007

[10] G.-Q. Chen and E. F. Toro, Centered difference schemes for nonlinear hyperbolic equations, *J. Hyperbol. Differ. Eq.* **1**, 531–566, (2004).

[11] F. Coquel, K. El Amine and E. Godlewski, A numerical method using upwind schemes for the resolution of two-phase flows, *J. Comput. Phys.* **136**, 272–288, (1997).

[12] J. Cortes, On the construction of upwind schemes for non-equilibrium transient two-phase flows, *Comput. Fluids* **31**, 159–182, (2002).

[13] J. Cortes, A. Debussche and I. Toumi, A density perturbation method to study the eigenstructure of two-phase flow equation systems, *J. Comput. Phys.* **147**, 463–484, (1998).

[14] G. Dal Maso, P. G. LeFloch and F. Murat, Definition and weak stability of nonconservative products, *J. Math. Pures Appl.* **74**, 483–548 (1995).

[15] F. De Vuyst, Stable and accurate hybrid finite volume methods based on pure convexity arguments for hyperbolic systems of conservation law, *J. Comput. Phys.* **193**, 426–468, (2004).

[16] S. Evje and T. Flåtten, Hybrid flux-splitting schemes for a common two-fluid model, *J. Comput. Phys.* **192**, 175–210, (2003).

[17] S. Evje and T. Flåtten, Hybrid central-upwind schemes for numerical resolution of two-phase flows, *ESAIM: M2AN* **29**, 253–273, (2005).

[18] S. Evje and T. Flåtten, Weakly implicit numerical schemes for a two-fluid model, *SIAM J. Sci. Comput.* **26**, 1449-1484, (2005).

[19] S. Evje and T. Flåtten, On the wave structure of two-phase flow models, *SIAM J. Appl. Math.* **67**, 487–511, (2007).

[20] M. Grandotto and J. Cortes, A three-dimensional transient two-phase flow analysis with a density perturbation finite volume method, *Int. J. Comput. Fluid D.* **19**, 311–319, (2005).

[21] J-M. Hérard and O. Hurisse, A simple method to compute standard two-fluid models, *Int. J. Comput. Fluid D.* **19**, 475–482, (2005).

[22] D. I. Ketcheson and A. C. Robinson, On the practical importance of the SSP property for Runge-Kutta time integrators for some common Godunov-type schemes, *Int. J. Numer. Meth. Fluids.* **48**, 271–303, (2005).

[23] M. Larsen, E. Hustvedt, P. Hedne, and T. Straume, Petra: A novel computer code for simulation of slug flow, in *SPE Annual Technical Conference and Exhibition*, SPE 38841, p. 1–12, October 1997.

[24] P. D. Lax, On the notion of hyperbolicity, *Comm. Pure Appl. Math.* **33**, 395–397, (1980).

[25] R. J. LeVeque, *Finite Volume Methods for Hyperbolic Problems*, Cambridge University Press, Cambridge, UK, (2002).

[26] S. T. Munkejord, S. Evje and T. Flåtten, The multi-stage centred-scheme approach applied to a drift-flux two-phase flow model, *Int. J. Numer. Meth. Fl.* **52**, 679–705, (2006).

[27] S. T. Munkejord, Comparison of Roe-type methods for solving the two-fluid model with and without pressure relaxation, *Comput. Fluids* **36**, 1061–1080, (2007).

[28] M. L. Muñoz-Ruiz and C. Parés, Godunov methods for nonconservative hyperbolic systems, *ESAIM: M2AN Math. Model. Numer. Anal.* **41**, 169–185, (2007).

[29] S. Noelle, N. Pankratz, G. Puppo and J. R. Natvig, Well-balanced finite volume schemes of arbitrary order of accuracy for shallow water flows, *J. Comput. Phys.* **213**, 474–499, (2006).

[30] S. Osher, Convergence of generalized MUSCL schemes, *SIAM J. Numer. Anal.* **22**, 947–961, (1985).

[31] H. Paillère, C. Corre and J. R. Carćía Gascales, On the extension of the AUSM+ scheme to compressible two-fluid models, *Comput. Fluids* **32**, 891–916, (2003).

[32] C. Parés and M. Castro, On the well-balance property of Roe's method for nonconservative hyperbolic systems. Applications to shallow-water systems, *ESAIM: M2AN Math. Model. Numer. Anal.* **38**, 821–852, (2004).

[33] C. Parés, Numerical methods for nonconservative hyperbolic systems: A theoretical framework, *SIAM J. Numer. Anal.* **44**, 300–321, (2006).

[34] V. H. Ransom, Faucet Flow, In: G. F. Hewitt, J. M. Delhaye and N. Zuber, editors, *Numerical Benchmark Tests*, volume 3 of *Multiphase Science and Technology*, pages 465–467. Hemisphere/Springer, Washington, USA, (1987). ISBN 0-89116-561-4.

[35] H. B. Stewart and B. Wendroff, Review article; two-phase flow: Models and methods, *J. Comput. Phys.* **56**, 363–409, (1984).

[36] J. H. Stuhmiller, The influence of interfacial pressure forces on the character of two-phase flow model equations, *Int. J. Multiphase Flow* **3**, 551–560, (1977).

[37] I. Tiselj and S. Petelin, Modelling of two-phase flow with second-order accurate scheme, *J. Comput. Phys.* **136**, 503–521, (1997).

[38] WAHA3 Code Manual, *JSI Report IJS-DP-8841*, Jožef Stefan Institute, Ljubljana, Slovenia, (2004).

[39] V. A. Titarev and E. F. Toro, MUSTA schemes for multi-dimensional hyperbolic systems: analysis and improvements, *Int. J. Numer. Meth. Fl.* **49**, 117–147, (2005).

[40] E. F .Toro and S. J. Billett, Centred TVD schemes for hyperbolic conservation laws, *IMA J. Numer. Anal.* **20**, 47–79, (2000).

[41] E. F. Toro, Riemann solvers with evolved initial conditions, *Int. J. Numer. Meth. Fl.* **52**, 433–453, (2006).

[42] E. F. Toro, MUSTA: A multi-stage numerical flux, *Appl. Numer. Math.* **56**, 1464–1479, (2006).

[43] E. F. Toro and V. A. Titarev, MUSTA fluxes for systems of conservation laws, *J. Comput. Phys.* **216**, 403–429, (2006).

[44] I. Toumi, An upwind numerical method for two-fluid two-phase flow models, *Nucl. Sci. Eng.* **123**, 147–168, (1996).

[45] I. Toumi and A. Kumbaro, An approximate linearized Riemann solver for a two-fluid model, *J. Comput. Phys.* **124**, 286–300, (1996).

[46] J. A. Trapp and R. A. Riemke, A nearly-implicit hydrodynamic numerical scheme for two-phase flows, *J. Comput. Phys.* **66**, 62–82, (1986).

[47] B. van Leer, Towards the ultimate conservative difference scheme II. Monotonicity and conservation combined in a second-order scheme, *J. Comput. Phys.* **14** 361–370, (1974).

[48] B. van Leer, Towards the ultimate conservative difference scheme IV. New approach to numerical convection, *J. Comput. Phys.* **23**, 276–299, (1977).

[49] B. van Leer, Towards the ultimate conservative difference scheme V. A second-order sequel to Godunov's method, *J. Comput. Phys.* **32**, 101–136, (1979).

[50] Y. Xing and C.-W. Shu, High order finite difference WENO schemes with the exact conservation property for the shallow water equations, *J. Comput. Phys.* **208**, 206–227, (2005).

[51] Y. Xing and C.-W. Shu, High-order well-balanced finite difference WENO schemes for a class of hyperbolic systems with source terms, *J. Sci. Comput.* **27**, 477–494, (2006).